# MAGNETIC MICROFLUIDIC PLATFORM FOR BACTERIA ISOLATION AND DETECTION

A THESIS SUBMITTED TO
THE GRADUATE SCHOOL OF ENGINEERING AND SCIENCE
OF BILKENT UNIVERSITY
IN PARTIAL FULFILLMENT OF THE REQUIREMENTS FOR
THE DEGREE OF
MASTER OF SCIENCE
IN
MECHANICAL ENGINEERING

By
Zahra Babaie
July 2023

Magnetic microfluidic platform for bacteria isolation and detection
By Zahra Babaie
July 2023

We certify that we have read this thesis and that in our opinion it is fully adequate, in scope and in quality, as a thesis for the degree of Master of Science.

Barbaros Çetin(Advisor)

Güneş Kibar(Co-Advisor)

Yegan Erdem

Veli Cengiz Özlap

Approved for the Graduate School of Engineering and Science:

Orhan Arıkan
Director of the Graduate School

# ABSTRACT

## MAGNETIC MICROFLUIDIC PLATFORM FOR BACTERIA ISOLATION AND DETECTION

Zahra Babaie
M.S. in Mechanical Engineering
Advisor: Barbaros Çetin
Co-Advisor: Güneş Kibar
July 2023

*S. pneumoniae* is widely recognized as a leading cause of respiratory infections worldwide, often resulting in high mortality rates. However, the advent of microfluidic technologies has brought significant advancements, including the simplified, sensitive, cost-effective, and rapid approach to pneumococcal bacteremia detection. In this study, we have revised the microfluidic magnetic platform patented by our research group to isolate the bacteria using synthesized micro-magnetic beads bonded with aptamer. In the initial phase of the experiments, the inlet flow rate was adjusted to match the rotational speed of the magnetic unit to retain the micro-magnetic beads within the fabricated microfluidic channel effectively. Subsequently, a series of experiments were conducted to assess microfluidics-based bacteria isolation at various flow rates, involving seven different concentrations of bacteria, and the outcomes were compared with those obtained through batch-type isolation method. The isolation selectivity of target bacteria from complex samples was also assessed with control bacteria at two different concentrations. Furthermore, the isolated micro-magnetic beads-bacteria complexes were also transferred to interdigitated microelectrodes unit for electrochemical impedance spectroscopy analysis. The ultimate objective is to integrate the isolation and detection components on the same microfluidic platform which leads to a rapid and precise diagnosis of bacterial infections.

*Keywords:* Microfluidics, bacteria isolation, micro-magnetic beads.

# ÖZET

# TÜRKÇE BAŞLIK

Zahra Babaie
Makine Mühendisliği, Yüksek Lisans
Tez Danışmanı: Barbaros Çetin
İkinci Tez Danışmanı: Güneş Kibar
Temmuz 2023

*S. pneumoniae*, dünya genelinde solunum yolu enfeksiyonlarının önde gelen nedenlerinden biri olarak görülmekte ve genellikle yüksek ölüm oranlarına yol açmaktadır. Ancak, mikroakışkan teknolojilerin ortaya çıkmasıyla, pnömokok bakteremisinin tespitine yönelik basitleştirilmiş, hassas, maliyet etkin ve hızlı bir yaklaşım gibi önemli ilerlemeler kaydedilmiştir. Bu çalışmada, araştırma grubumuz tarafından daha önce patentlenen mikroakışkan manyetik platformu revize edilerek, sentezlenmiş mikro-manyetik parçacıklar üzerine uygun aptamerleri yerleştirerek bakteriyi izolasyonu için kullandıldı. Deneylerin başlangıç aşamasında, mikroakışkan kanal içerisindeki akış hızı yine kanallar içerisinde bulunan mikro-manyetikparçacıkların etkin bir şekilde kanal içerisinde tutulabilmesi için manyetik platfomun gerekli dönme hızı ayarlandı. Daha sonra, mikroakışkan tabanlı bakteri izolasyonu yedi farklı bakteri konsantrasyonu için farklı debilerde yapıldı ve elde edilen sonuçlar geleneksel izolasyon yöntemi ile karşılaştırıldı. Hedef bakterilerin karmaşık numunelerden izolasyon seçiciliği, iki farklı konsantrasyondaki kontrol bakterileriyle birlikte değerlendirildi. Ayrıca, izole edilmiş mikro-manyetik parçacık-bakteri kompleksleri, elektrokimyasal empadans spektroskopi analizi için mikroelektrot ünitesine transfer edildi. Çalışmamızın nihai amacı, izolasyon ve tespit bileşenlerini ayni mikrakışkan platformda entegre ederek bakteriyel enfeksiyonların hızlı ve kesin tanısını sağlamaktır.

*Anahtar sözcükler*: Mikroakışkan sistemler, bakteri izolasyonu, mikro manyetik parçacıklar.

# Acknowledgement

I am deeply grateful to my thesis supervisor, Assoc. Prof. Barbaros Çetin, for his unwavering support, expert guidance, and valuable feedback throughout the entire research process. I would like to express my gratitude to Assist. Prof. Güneş Kibar (my co-advisor) and Prof. Veli Cengiz Özalp for their contributions and feedback on my thesis. Their insights have greatly improved the quality of this thesis.

Completing this thesis has been an incredible journey, and it wouldn't have been possible without the constant support of my love, Behnam. His love, motivation, and sacrifices, even across distances, have been the driving force behind my success, and for that, I am eternally grateful for his presence in my life.

To my entire family, my parents, brother, and sister, I want to express my heartfelt appreciation for being the unwavering foundation of love and support in my life. Even from afar, their presence has been a constant source of comfort and inspiration.

From the depths of my heart, I extend my heartfelt gratitude to my dear friends, Amna and Momil, who have become like family to me during my time at Bilkent. Their love, understanding, and encouragement have been a constant source of strength and inspiration. I am truly blessed to have such incredible friends by my side, making my journey here all the more meaningful and memorable.

I would like to express my sincere appreciation to my colleagues and friends, with a special mention to Ege Cura, our undergraduate lab member, for his invaluable support and contributions to this study.

Thank you all for being an integral part of this academic journey.

I would also like to thank Turkish Scientific and Technical Council (TÜBİTAK) for the financial support of my thesis through the project 220N316.

# Contents

# List of Figures

# List of Tables

# Chapter 1

# Introduction

*Streptococcus pneumoniae (S. pneumoniae)* is responsible for a significant proportion of community-acquired pneumonia (CAP) cases in adults, with 30 to 70 % needing hospitalization. This bacteria is a gram-positive, spherical bacterium that is often observed in pairs [1]. This type of bacteria is considered as a significant cause of bacteremia, meningitis, upper respiratory tract infections, and otitis media around the world [2]. Yearly, more than 400 million infected cases with one million deaths are reported [3]. Despite the development of a 13-valent pneumococcal conjugate vaccine (PCV), some specific cases still have high morbidity and mortality rate [4]. Currently, the diagnosis of pneumococcal bacteremia relies on conventional bacterial culture with bacterial isolation from specimens and the usual time of *S. pneumoniae* detection (or more general bacteria detection) in a blood culture takes 24 to 48 h [5]. The other methods of detection are the PCR-based nucleic acid amplification test (NAAT) and immunochromatography assay (ICA). While these methods are rapid and accurate, NAAT is expensive and requires specific equipment. In ICA, the chance of a misdiagnosis is high, and it has a limited sensitivity [3]. Hence, it is crucial to create straightforward, highly responsive, cost-effective, and rapid techniques to identify *S.pneumoniae*.

## 1.1 Background information on microfluidics

Microfluidic chips, also known as lab-on-a-chip devices, have gained popularity as they offer an opportunity for integrated platform which can handle various laboratory operations such as sample preparation, reactions, separation, and detection on a microchip [6, 7]. Terry [8] first introduced the concept of a microfluidic chip analysis in 1979 with his development of a miniature gas analysis system on a silicon wafer utilizing photolithography and chemical etching techniques.

The most significant advantage of a microfluidic system is the flexible combination of a controllable micro-environment in which the microfluidic flow can accurately be driven and controlled in microchannels, improving detection sensitivity and the efficiency of interaction [9, 10]. In contrast to conventional approaches, microfluidic chips offer several benefits, including miniaturization, improved throughput, rapid analysis, integration of multiple functions, and reduced consumption [11]. In recent years, there has been a significant advancement in the development and application of microfluidic devices in different fields such as bioparticle manipulation [7, 12–17], chemical reactors for micro/nanoparticle synthesis [18, 19] etc. The advent of microfluidic platforms has brought about a revolution in the study of unculturable environmental species by eliminating the necessity for pre-analysis culturing [20, 21]. Microfluidic devices have proven to be suitable for manipulating the microscale environment, making them powerful tools for studying bacteria [22, 23].

Choice of material is a crucial step in the fabrication of microchips. In order to attain diverse functionalities, the utilization of materials possessing particular traits such as hardness, conductivity, hydrophobicity, light transmission, corrosion resistance, process feasibility, and biocompatibility is frequently required [24]. Microfluidic materials can be categorized into organic materials [25], polymer materials [26], hydrogel [27], and paper [28]. The physicochemical properties of inorganic materials impose limitations on their applications in biological research. Consequently, polymer-based materials have predominantly been utilized in this field due to their ease of surface modification, improved biocompatibility [29], and

the emergence of novel chip fabrication techniques. In various fields, traditional inorganic materials have been substituted with a diverse selection of natural and synthetic polymer materials, which encompass thermoplastic and thermosetting polymers [30].

### 1.1.1 Inorganic materials

In the early stages of microfluidic chip development, silicon was commonly used due to its exceptional surface chemical properties, which made it well-suited for immobilizing ligands [31,32]. However, silicon's application is limited in observation methods because of its insufficient electrical insulation, high price, and poor transmittance [9]. Nowadays, glass and quartz have emerged as substitutes for silicon in microfluidic chips. Glass offers several advantageous properties, such as excellent electroosmotic behavior, transparency, biocompatibility, and ease of processing [33].

### 1.1.2 Polymer materials

In the field of biological analysis, there are still numerous constraints associated with the use of inorganic materials. Observing cells under a microscope while keeping them alive inside silicon microchips is challenging due to silicon materials' poor transparency and permeability. On the other hand, owing to their exceptional optical properties, chemical inertness, electrical insulation, and thermal characteristics [34], polymers have become the primary materials utilized in microfluidics for biological applications. Moreover, inexpensive organic materials offer the advantage of being easily processed through various methods, and different classes of polymers facilitate simpler surface modifications [35]. In general, these materials can be classified into three categories: silicone elastomers, thermosetting plastics, and thermoplastics.

**Silicone elastomer materials**, particularly PDMS (polydimethylsiloxane),

have emerged as the favored choice for fabricating microfluidic chips during the last decade [36]. PDMS has been widely used for microfluidic chip fabrication because of the possibility of rapid chip fabrication and producing transparent chips attached to the glass. The elastomer molding technique was initially developed by Bell Laboratories in the 1970s [37]. Subsequently, it found applications in fabricating microfluidic chips during the 1980s [38]. In the late 1990s, Whitesides *et al.* [39] introduced the soft lithography technique to produce microfluidic chips. Consequently, PDMS molding and soft lithography have become widely adopted methods for microfluidic chip fabrication. PDMS exhibits a low surface tension, making detaching the chip injection mold from the photoresist template easy. Additionally, PDMS has the ability to form permanent bonds with other PDMS or glass surfaces using methods like plasma oxidation or other alternatives. It possesses a significant capacity for elastic deformation [40] and can allow gas penetration, which is advantageous for cell culture [41]. In addition, PDMS exhibits a high level of transparency, facilitating the real-time visualization of organisms within microfluidic chips. Consequently, due to these notable properties, it has been widely employed as the primary material for microfluidic chips in various biological applications. Moreover, silicon elastomers exhibit deformability under external forces, allowing them to return to their original shape when the force is removed. This unique property enables the direct integration of micropumps and microvalves into the chip design, facilitating dynamic fluid control and manipulation within microfluidic systems [9]. Nevertheless, there are certain limitations to the application of PDMS. Its hydrophobic surface can lead to the undesired adsorption of biomolecules [42], and the porous structure within PDMS can lead to water molecule evaporation and alter solution concentrations. Additionally, when constructing multilayer channels, the flexibility of the material can result in the collapse and subsequently hinder the large-scale production, leading to commercial setbacks [9].

**Thermosetting plastics** are utilized in microfluidic chip fabrication. These materials undergo a process known as cross-linking, where the polymer chains form a network structure that grants the bulk material heat resistance. Once the cross-linking network is established, reshaping the material becomes difficult.

Additionally, the cross-linking network in thermosetting polymers imparts remarkable mechanical strength, leading to increased material stiffness. Typically, these materials exhibit stability at high temperatures and show resistance to a wide range of solvents. Moreover, they possess the capability to transmit visible light. With appropriate bonding methods available, it is feasible to construct microfluidic chips entirely from thermosetting materials. An example of such a thermosetting plastic is SU-8 photoresist, commonly employed in soft lithography techniques, which allows for genuine 3D microfabrication through photopolymerization [43]. Thermosetting materials offer superior strength, enabling their application in the creation of structures with high aspect ratios and the ability to stand freely [44].

**Thermoplastics** can be reshaped at high temperatures, unlike thermosetting plastics. Common thermoplastics such as polycarbonate (PC), polystyrene (PS), polytetrafluoroethylene (PTFE), polymethyl methacrylate (PMMA), and polyethylene terephthalate (PET) are frequently employed for observing cells in microfluidic systems. However, there are limitations to the use of thermoplastic materials in microfluidic chip fabrication. They are not tolerant organic solvents like alkanes, and their inadequate air permeability makes them unsuitable for long-term cell culture applications. Moreover, thermoplastics often require complex processing, leading to rigid structures after molding and higher manufacturing costs [45]. As a result, thermoplastics are not widely utilized in the fabrication of microfluidic devices [9].

**Hydrogel** is created by cross-linking a hydrophilic polymer chain in a water-based environment, resulting in a three-dimensional structure. This material has a porous arrangement that facilitates the diffusion of biomolecules and small molecules. As a result, hydrogels have a significant water content, which enhances effective mass transport, fosters better cell viability, and encourages cell proliferation. Both natural and synthetic hydrogels have found applications as biomaterials in microfluidic devices [9]. Synthetic polymers such as polyethylene glycol and polylactic acid are commonly employed in microfluidic devices. On the other hand, natural polymers like collagen, calcium alginate [46] gelatin, cellulose, and chitosan have been extensively utilized as biomaterials in microfluidic

applications. Gel materials are typically compatible with biological systems, although the level of cell adhesion to various gels varies based on the origin of the gel material. Some gels lack specific sites for cell adhesion, resulting in a relatively weak interaction between the gel material and cells [9].

### 1.1.3 Methods for capturing specific pathogenic bacteria

Various strategies have been employed to enhance the selective detection of target bacteria from complex samples. These include utilizing antibody-antigen interactions, aptamer binding, bacteriophage biological recognition, capture using antibiotics or antimicrobial peptides, and other interactions involving target recognition. These approaches are frequently implemented in microfluidic chips [47].

**Antibody-antigen** interactions are prevalent methods for capturing bacteria from diverse, complex samples in microfluidic devices [48, 49]. The antibody-antigen sandwich approach is commonly employed in microfluidic biosensors to capture intact bacterial cells without the need for cell lysis or enzyme release, which is typically required in techniques like ELISA for subsequent signal amplification and transduction. Antibodies have good specificity and selectivity, but their stability is low, and they are expensive [47].

**Aptamers** have gained significant popularity in recent years as a means of recognizing and binding to analytes [50]. They are synthetic DNA or RNA probes that are generated in vitro through a selection method known as Systematic Evolution of Ligands by Exponential Enrichment (SELEX) [51]. Aptamers offer several advantages, including precise synthesis, easy modification, high purity, smaller molecular weight (approximately 12-30 kDa), and lower cost. They also exhibit improved thermo/pH stability, making them suitable for easy storage [50, 52].

**Antimicrobial peptides (AMPs)** are small peptide fragments, typically

composed of fewer than 40 amino acid residues, and are found in various organisms. These peptides play a crucial role in the innate immune system, serving as a defense mechanism to protect the host from pathogens [53]. They are cheap, can simply be synthesized, and have high stability [54]. Moreover, the ideal AMP molecule can be selected from existing databases since their sources contain a wide range, unlike antibodies and aptamers. However, most current AMP-mediated microfluidic platforms require microscopy, making them less sensitive and more complicated to operate [55].

**Bacteriophage biology recognition (Phages)**, also known as phages, possess the ability to specifically target and infect bacteria by exploiting their metabolic machinery [56]. Bacteriophages offer a promising alternative to traditional molecular probes in the development of highly specific, sensitive, stable, rapid, selective, cost-effective, easily accessible, and reliable detection platforms for pathogenic bacteria [47]. However, following the fixing onto a sensor's surface, phages dry out and loose their activity. The large size of the phages leads to the decrement of measurement signals [55].

**Antibiotics** can interact with bacterial cell walls, making them viable capture elements. For instance, vancomycin can form a robust hydrogen bond by binding to the amine group of peptidoglycan on bacteria cell walls using its carbonyl group. Recently, nanomaterials modified with vancomycin have been employed to isolate and detect both gram-positive (GPB) and gram-negative (GNB) bacteria [47].

### 1.1.4 Detection methods for bacteria

Bacterial detection spans various domains, such as food safety, agricultural and sideline product manufacturing, and the prevention and management of foodborne illnesses, among other areas. As a result, it is essential to establish a method for rapid and sensitive bacterial detection to diagnose and treat diseases at their early stages. Conventional approaches to bacterial detection, such as plate colony counting, multi-tube fermentations, and filter membrane techniques, are

characterized by time-consuming processes with limited efficiency. In contrast, microfluidic devices can integrate compatible biogeochemical units for bacteria detection. Microfluidic bacteria detection can be generally categorized into three groups optical, electrochemical, and biology-based [9].

#### 1.1.4.1 Optical-based detection method

Optical microfluidic detection techniques include laser-induced fluorescence, chemiluminescence, immunofluorescence, bioluminescence, Raman spectroscopy, and thermal permeation microscopy. Among these techniques, fluorescence and chemiluminescence have been widely utilized for the detection of bacteria [9].

- **Fluorescent analytical strategies** have emerged as highly promising techniques for quantitative detection in microfluidic biosensors used for bacterial detection. These strategies offer a comprehensive response range and exceptional sensitivity, positioning them as ideal candidates for such applications. In biosensors, functionalized nanoparticles such as gold nanoparticles (AuNPs) and graphene oxide are frequently used as acceptors and donor fluorophores instead of traditional organic dyes. This choice is motivated by the limitations of organic dyes, including limited absorption range, broad emission range, and susceptibility to photobleaching. By utilizing functionalized nanoparticles, biosensors can overcome these limitations and achieve improved performance in terms of fluorescence detection [47].

- **Chemiluminescence (CL)** eliminates the need for an excitation light source, thereby eliminating noise and background emission. In addition to its ability to selectively target specific substances, it offers high sensitivity for trace analysis. As a result of these benefits, microfluidic chemiluminescence has been employed in bacterial analysis [57].

  **Immunofluorescence** involves the fusion of particular antigen-antibody interactions, fluorescent tagging, and a fluorescence microscope, allowing for the qualitative or quantitative identification of bacteria [9].

- **Colorimetric detection** is favorable since it provides the chance of observation by the naked eye. Transforming the bio-recognition signal into color variations is the main challenge of this method, and two primary tools are chromogenic substrates and enzymes [47]. TMB coloration assays, which rely on catalysis assays [51], and immunochromatography assays using AuNPs, are commonly employed in visual detection systems [58].
- **Surface-enhanced Raman spectroscopy (SERS)** has become an effective method for detecting bacteria since it can obtain molecular fingerprint information with a non-destructive and on-line qualitative nature [47].

#### 1.1.4.2 Electrochemical method

The development of electrochemical biosensors has facilitated the detection of pathogens in different matrices without the need for sample preparation. This feature makes them well-suited for rapid, on-site pathogen detection [59–61]. Electrochemical chips offer a sensitive and rapid approach for bacterial detection. By applying negative pressure to pass bacterial suspensions through the test hole, diverse pulse signals are generated as a result of variations in bacterial sizes and surface properties. These signals are subsequently amplified, sorted, and converted into relevant information regarding the quantity and types of bacteria [9].

**Electrical impedance technique (EIT)** identifies microbes based on their metabolic activities. It has also been applied to microfluidics systems. The required concentration for bacterial detection decreases while the sensitivity for the electrical impedance chip increases compared to the traditional impedance method. Compared to other analytical technologies, impedance biosensors typically require simpler devices, allowing for easier integration with electronic reading devices. Furthermore, they tend to be less susceptible to environmental impacts and pollution, making them a robust choice for various applications [62]. The utilization of electrical impedance chips offers several advantages in bacterial detection, including the ability to detect bacteria at lower concentrations and

enhanced sensitivity compared to traditional impedance methods. The combination of diverse electrode options and the personalized design of microfluidic chips presents a promising research direction for the future of electric impedance chips [9].

#### 1.1.4.3 Biology-based detection method

The progress in biological technology has given rise to gene chips and biosensors as novel approaches in bacterial detection. These technologies offer new approaches for analyzing and identifying bacterial pathogens. Microfluidic gene chips have been extensively utilized for analyzing bacteria. These chips enable the analysis of both target proteins and nucleic acid-based biomarkers. [9].

- **Polymerase chain reaction (PCR)** stands as the extensively utilized and the most dependable and precise method for nucleic acid analysis. Integrating microfluidic devices with PCR offers the advantages of enhanced throughput, minimal material consumption, and the ability to accommodate multiple analysis modules within a shorter timeframe [9].

- **Loop-mediated isothermal amplification (LAMP)** has undergone advancements and found application as a rapid, sensitive, and specific method for bacterial detection. Compared to PCR, LAMP does not require a thermal cycler and demonstrates higher tolerance towards inhibitory components found in crude samples. So, it has successfully been applied in bacteria and virus detection with promising clinical applications. In addition, the new trend of combining LAMP technology with a microfluidic chip can provide a constant temperature for amplification in a short time and an easy way of operation [9].

- **Enzyme catalytic reaction sensors** on a chip can reduce the sample and reagent consumption within a shorter time so that they reduce the cost of detection. These sensors employ immobilized enzymes on channel surfaces or electrodes to convert enzymatic catalytic reactions into specific

detectable signals. Currently, enzyme catalytic sensors find extensive application in detecting blood sugar, urea, and cholesterol levels [9].

- **Immunosensors** rely on the specific recognition between antigens and antibodies to detect bacteria. The signals generated by this interaction can be converted into changes in resistance, current, or refractive index. These microfluidic-based sensors are predominantly employed for the detection of pathogens, bacteria, and viruses [9].

## 1.2 Literature review

Understanding the customary and recognized levels of bacteria is crucial for the development of point-of-care diagnostic devices. However, it should be noted that the criteria for defining toxic levels vary based on the specific type of bacteria.

The isolation of pathogens from samples has been investigated using diverse methodologies. Microfluidic-based bacteria isolation is one of them [49, 63]. Chang *et al.* [64] could effectively identify viable bacteria within samples of periprosthetic joint infection (PJI) using a microfluidics platform for the first time. By employing a microfluidic system, they were able to differentiate the presence of viable bacteria within a time frame of an hour, achieving a limit of Detection (LOD) of $10^4$ colony-forming units (CFU). Faridi *et al.* [65] separated *E. coli* from undiluted whole blood at an efficiency of 76% using an elasto-inertial microfluidic device. In addition, there are several studies that utilized elasto-inertial microfluidic devices to isolate different types of bacteria [66–68].

Microfluidic chips integrated with PCR [69] and LAMP [70, 71] have been employed to analyze different types of bacteria. Azizi *et al.* [72] combined droplet-based microfluidics and LAMP to create a highly sensitive biosensor to amplify extracted RNA templates for the purpose of detecting *Salmonella typhimurium*. Droplet microfluidics also combined with PCR to isolate various bacteria and achieved a high throughput by processing a maximum of 80 samples per hour within a single reactor [73]. Choo *et al.* [74] introduced a viscoelastic microfluidic

system to concentrate bacterial cells continuously. They analyzed the cells using flow cytometry and real-time LAMP (RT-LAMP) and calculated the recovery rate of 51.6%. In the study by D'Amico *et al.* [75], membraneless microfluidic dialysis and dielectrophoresis were included within a microfluidic system to achieve the label-free isolation and concentration of bacteria from whole blood. The integrated system isolated approximately 79±3% of *E.coli* and 78±2% of *S.aureus* from whole blood. Li *et al.* [76] presented a study where they utilized an acoustofluidic device to isolate *E. coli* from human blood samples. The device capitalized on the disparity in size between *E. coli* and blood cells, achieving a purity level of over 96%. Dow *et al.* [77] developed a microfluidic chip made of polystyrene that was created and utilized as an acoustic separator to purify bacteria from whole blood. The system successfully achieved a yield of 40-60% for the spiked bacteria while effectively depleting 85-95% of red blood cells. Electrophoresis [78], Isotachophoresis (ITP) [79], and Impedimetric [80] detection methods were combined with a microfluidic system for concentrating pathogens prior to analysis without compromising their viability. Table 1.1 provides a comprehensive overview of various bacterial isolation techniques integrated with microfluidic systems.

Wu *et al.* [81] simulated the motion of the magnetic bead by the Lagrangian tracking method and calculated the separation efficiency. The findings indicated that both L-turning/T-junction microchannels exhibited greater separation efficiency than the conventional straight-microchannel separator. Beyor *et al.* [82] developed the microfluidics system to isolate *E. coli K12* efficiently with low concentrations. They introduced two notable enhancements compared to previously published systems. Firstly, extending the channel length and placing the magnets after each bifurcation provided uniform distribution of beads across all parallel channels. Additionally, they implemented multiple flutter steps to allow the solution to pass over the bead bed multiple times within a single pass. These enhancements yielded substantial improvements in capture performance, achieving an impressive efficiency of 70%. In addition to examining channel geometry and flow properties, the researchers also investigated the influence of alterations in the magnetic field within the channel on the capture of magnetic beads. Munir

*et al.* [83] performed the mathematical model to predict the transport and capture of the magnetic nanoparticles in a microfluidic device enclosed by a permanent magnet and investigated the effect of inlet velocities, diameter particles, and strength of magnetic field on the trapping efficiency. Xia *et al.* [84] introduced a microfluidic device incorporated with a high-gradient magnetic field concentrator (HGMC) at one side of a microfluidic channel. By employing this microdevice, they effectively eliminated living *E. coli* bacteria bound to magnetic nanoparticles (MNPs) from solutions with red blood cells and reached a maximum of about 92% separation efficiency for 1.6 μm mMBs. Weng *et al.* [3] developed the magnetic microfluidic combined with the Enzyme-linked immunosorbent assays (ELISAs) process for detection of *S. pneumoniae*. Microfluidic ELISAs offered the advantage of reducing the need for manual handling and significantly decreasing operation time. Rodoplu *et al.* [85] employed streptavidin-modified superparamagnetic microbeads to detect *E. coli* expressing the green fluorescent protein (GFP). The researchers successfully determined the limit of detection and limit of quantification values for *E. coli* as 2 CFU/mL and 10 CFU/mL, respectively. A simple and straightforward approach was devised by Lee *et al.* [86] for the detection of pathogenic bacteria, involving the use of magnetic nanoparticle clusters (MNCs) in conjunction with a 3D-printed helical microchannel. The concentration of *E. coli* bacteria was assessed using a light absorption spectrometer, revealing a limit of detection of 10 CFU/mL in buffer solution and 100 CFU/mL in milk. In another study, Lee *et al.* [87] developed a novel 3D immunomagnetic flow assay for rapid detection of pathogenic bacteria by immobilizing antibody-functionalized magnetic nanoparticle clusters (AbMNCs) on the surfaces of 3D-printed cylindrical microchannel. The detection sensitivity of their system surpassed 10 CFU/mL, and the entire assay, encompassing binding, rinsing, and detection steps for a 10 mL sample, was completed in under 3 minutes. More studies on the selective isolation of the bacteria with microfluidic system were discussed in the literature [88–91]. In addition, several other methods utilized magnetic beads [92–95] and magnetic silica nanotubes (MSNTs) [96] for bacterial detection. The summary of the literature review is given in Table 5.1.

Table 1.1: Various bacteria isolation literature.

| **Microfluidic** | | | |
|---|---|---|---|
| **Authors** | **Bacteria type** | **Mechanism** | **Process time** |
| Zelenin *et al.* [63] | *E.coli, M.luteus* | Microfluidic-based | NG |
| Afbagi *et al.* [49] | *E.coli* | 3DpmμFD+PCR+ Electrophoresis | 50 mins |
| Chang *et al.* [64] | *E.coli* | Integrated microfluidic | NG |
| Faridi *et al.* [65] | *E.coli* | Elasto-inertial | NG |
| Yao *et al.* [66] | *Salmonella* | Viscoelastic inertial | 1h |
| Condiana *et al.* [67] | *S.pastorianus, S.cerevisiae* | Inertial+ mass spectrometry | 20-90 mins |
| Iyengar *et al.* [68] | *E.coli, S.Capitis* | Elasto-inertial | 40 mins |
| Jiang *et al.* [69] | *K.pneumoniae, S.aureus, E. coli P.aeruginosa, E.faecalis* | PCR | 2.5 h |
| Jiang *et al.* [70] | *S.aureus, E.coli, P.aeruginosa C. koseri, K. pneumonia* | LAMP | 1.5 h |
| Jin *et al.* [71] | 10 waterborne bacteria | LAMP | 85 mins |
| Azizi *et al.* [72] | *Salmonella* | Droplet+ LAMP | NG |
| Peham *et al.* [73] | *S.aureus, E. coli, P.aeruginosa* | Droplet+ PCR | NG |
| Yu *et al.* [97] | *S.aureus, E. coli* | Integrated system | 1h |
| Choo *et al.* [74] | *S.aureus* | Viscoelastic + RT-LAMP | NG |
| D'Amico *et al.* [75] | *E. coli, S.aureus* | Dialysis+Dielectrophoresis | 1h |
| Li *et al.* [76] | *E.coli* | Acoustofluidic | NG |
| Dow *et al.* [77] | *P.aeruginosa, S.aureus,E. coli* | Acoustophoresis | NG |
| P-Enengl *et al.* [78] | *E. coli* | Electrophoresis | <27 mins |
| Schwartz *et al.* [79] | *E. coli* | ITP+ Electrophoretic | > 1h |
| Wang *et al.* [80] | *E. coli* | Impedimetric | 1h |

Table 1.2: Various bacteria isolation using mMBs in literature.

| **Microfluidic** | | | |
|---|---|---|---|
| **Authors** | **Bacteria type** | **Mechanism** | **Process time** |
| Xia *et al.* [84] | *E.coli* | Micromagnetic | NG |
| Weng *et al.* [3] | *S.pneumoniae* | MMF-ELISA | 12 mins |
| Rodoplu et al. [85] | *E.coli* | Magnetic-assisted+Fluorescence | 1h |
| Lee *et al.* [86] | *E.coli* | MNCs | NG |
| Lee *et al.* [87] | *Salmonella* | AbMNCs+ ATP luminescence | 3 mins |
| Pivetal *et al.* [88] | *E.coli, Acinetobacter* | probe-based cell fishing | NG |
| Pereiro *et al.* [89] | *S.enterica, E.coli, E. cloacae* | Magnetic | 2-8 h |
| Miller *et al.* [90] | *E.coli* | mMBs +Electroosmotic | NG |
| Kim *et al.* [91] | *E.coli* | MNPs | NG |
| **Other Methods** | | | |
| Poncelet *et al.* [92] | *E.coli* | suspendedMNP | NG |
| Lee *et al.* [93] | *E.coli, V. parahemolyticus Salmonella, L. monocytogenes* | Virtual Net+ATP luminescence | 15 mins |
| Lee *et al.* [94] | *E.coli* | Virtual filters with MNPs | $<$ 2h |
| Huang *et al.* [95] | *E.coli, Salmonella* | capillary | NG |
| Nguyen *et al.* [96] | *S.typhimurium* | MSNTs+Impedimetric | 30 mins |

NG →Not Given

## 1.3 Objectives and motivation

*S.pneumoniae* is a leading cause of respiratory infection with high mortality rates around the world, particularly among susceptible populations, including children, the elderly, and individuals with compromised immune systems. So, there is a growing urgency to discover rapid and effective techniques for the isolation and detection of this bacterium. Flow within microchannels allows precise control and manipulation of fluids at a small scale which enhances detection sensitivity and improves the efficiency of interactions within the system. In addition, the use of micro-magnetic beads (mMBs) enables precise capturing of a particular bacterial species and distinction among various bacterial types present in a sample.

In this study, we revised the patented magnetic platform from our research group [98] to isolate *S. pneumoniae* from PBS buffer solution and blood flow for different concentrations of bacteria. First, we synthesized the mMBs in the lab, followed by binding them with purchased aptamers to isolate the bacteria selectively. In the next step, electrical impedance spectroscopy (EIS) with fabricated gold electrodes was utilized to detect the bacteria. The final goal of this research is to combine two steps and produce fast, accurate biosensors to isolate *S. pneumoniae*.

## 1.4 Thesis outline

The theses outline is listed below:

**Chapter 2** begins by describing the design of a microfluidic chip that is compatible with our magnetic platform. Then the fabrication steps for the microfluidic chip and electrodes are defined in detail. Next, the magnetic particle synthesizing procedure and its characteristics are included. Finally, the method for immobilizing the selected aptamer on synthesized mMBs is explained.

**Chapter 3** deals with explaining the experimental setup and experiment procedure. The experiments are divided into two subsections. The first part focuses on retaining the mMBs inside the spiral channel by setting the flow rate and rotational speed of the magnetic unit. The second part demonstrates the experimental procedure for bath and microfluidic isolation of bacteria using modified mMBs followed by bacteria culturing and calculating the capture efficiency. Furthermore, the development of Interdigitated microelectrodes for electrochemical impedance spectroscopy (EIS) sensor for bacterial detection is discussed.

**Chapter 4** provides the results for the first and second parts of the experiments and compares the capture efficiency of the magnetic platform and batch bacteria isolation for different concentrations of the bacteria. Moreover, bacteria detection by the electrochemical impedance spectroscopy (EIS) method is discussed.

**Chapter 5** concludes the thesis by summarizing previous chapters, addressing method limitations, and suggesting improvements and future research directions.

# Chapter 2

# Fabrication

## 2.1 Microfluidic chip design

This study utilizes a spiral microfluidic device in conjunction with a rotating magnetic field to isolate bacteria. The length of the microfluidic channel is determined based on a previously proposed patent for DNA isolation [98], and the geometry is altered to comply with the sample loading unit, what we call flexible hydraulic reservoir (FHR) [99, 100] which was patented by our research group. FHR is an inexpensive, re-usable microfluidic component enabling zero-dead-volume sample injection into a microfluidic chip. In Figure 2.1, the schematic representation of the microfluidics channel employed in this research is depicted. The microfluidics chip is designed with two distinct inlets, denoted as "Inlet-1" and "Inlet-2." Inlet-1 is designated for injecting the bacteria solution, while Inlet-2 is intended for loading the washing buffer. The purpose of the washing buffer is to remove bacteria that have bonded with mMBs, subsequently carrying them to the detection unit for further analysis. However, in the context of our research, we have exclusively utilized Inlet-1, since the detection unit is placed on a separate chip. Both the bacteria solution and PBS buffer solution are loaded through this single inlet. The microchannel itself possesses a width of 400 μm and a height of 120 μm, and a volume of about 8 μL.

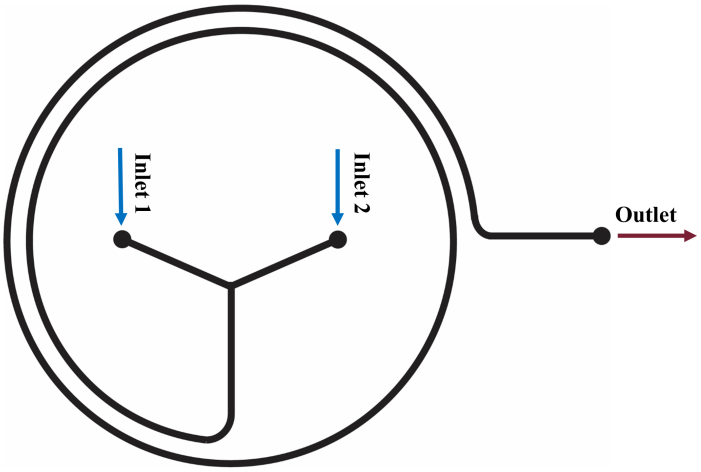


Figure 2.1: Schematic drawing of the microfluidic channel.

## 2.2 Microfluidic chip fabrication

To fabricate the master mold, a two-step soft-lithography procedure, as shown in Figure 2.2, is followed. First, a negative photoresist (SU-8 2005) is spin-coated on a cleaned 4-inch silicon wafer to create a thin adhesion layer for constructing subsequent structures. Later, the base layer is pre-baked on a hotplate before UV exposure and then post-baked at 95°C. In order to get the channel structure, a much thicker negative photoresist (SU-8 2050) is spin-coated on top of the base layer to reach the desired height. The resist is heated before the exposure for a longer time, followed by UV exposure using the chromium mask. Then, the patterned silicon wafer is backed on the hotplate before drowning to the SU-8 developer to remove unsolidified parts. Finally, the mold is washed with Isopropyl Alcohol (IPA) and Deionized water (DI) and dried with Nitrogen. The channel dimensions are confirmed by analyzing them with a laser microscope. The detailed fabrication steps are included in Appendix A.1. The fabricated master mold is covered with PDMS (Polydimethylsiloxane) and curing agent (Sylgard 184) with a ratio of 10:1. The mixture is left in the oven at 80°C to get cross-linked. The solid PDMS is peeled off and punched into the inlets and outlets. Afterward, it is bonded with clean (2”×3”) microscope slides using the plasma cleaner.

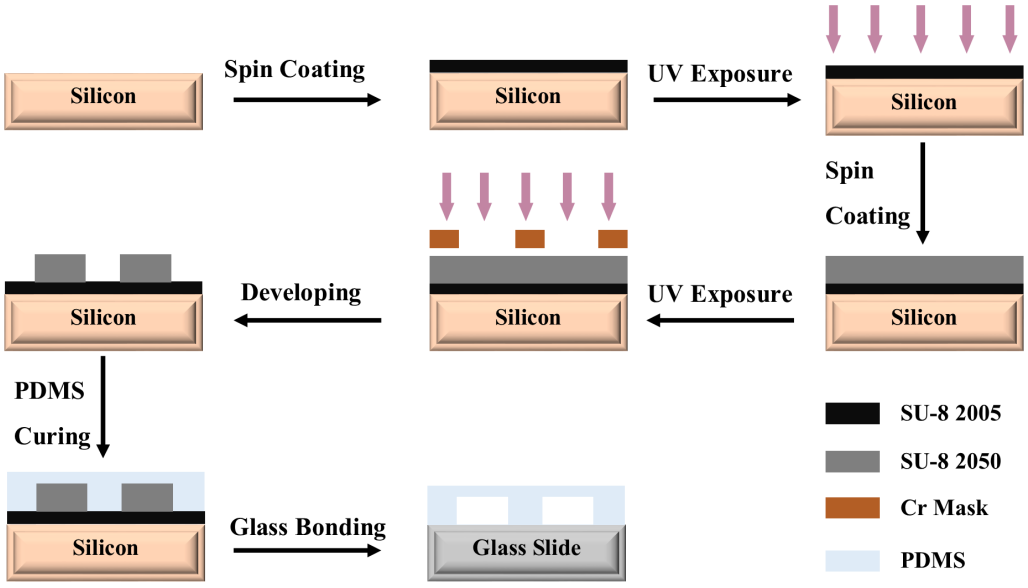


Figure 2.2: Fabrication steps of soft lithography to prepare the mold, PDMS molding with glass bonding.

## 2.3 Electrode fabrication

The fabrication of gold-interdigitated microelectrodes involves a series of steps utilizing photolithography and wet etching on a glass substrate. Each microelectrode consists of ten pairs of digit finger electrodes. These electrodes are characterized by a finger width of 20 μm, a finger length of 1.0 mm, and a thickness of 80 nm. The separation between neighboring finger electrodes measures 50 μm. In order to manufacture the Interdigitated Electrode (IDE) for bacteria detection, CAD software is employed to create a design to provide the chromium mask, which is required during the fabrication process. The following procedures, as shown in Figure 2.3, are employed to fabricate the electrodes. First, the clean glass wafer is spin-coated with positive photoresist (AZ5214) and then heated in an oven with a temperature of 120°C for 70 seconds. After that, the wafer is transferred to be exposed to UV light with a designed mask. Subsequently, the wafer is sunk in 4:1 water: AZ developer (400K) to remove the exposed regions. The developed pattern is placed in the thermal evaporator for metal deposition.

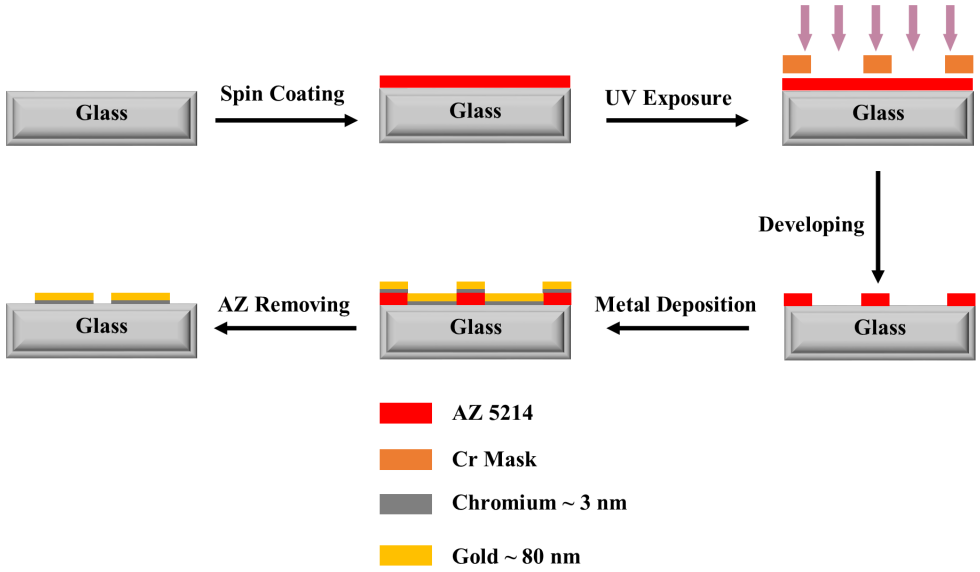


Figure 2.3: Fabrication steps for Interdigitated microelectrodes.

Initially, a very thin layer of chromium (3 nm) is deposited to increase the adhesion between gold, followed by gold deposition to reach the thickness of 80 nm under the controlled rate. In the final step, the wafer is immersed in Acetone to eliminate the AZ and obtain the electrodes. Appendix A.2 contains detailed electrode fabrication steps. The fabricated electrodes can be seen in Figure 2.4.

## 2.4 Particle synthesis for bacteria detection

Immunomagnetic bead-based separation is a widely adopted technique in microfluidic devices. This method utilizes mMBs coated with specific binding ligands that selectively bind to target biomolecules, enabling isolation of the mMB-complex within the system for further analysis [82, 101, 102]. The magnetic field is employed to capture and isolate the mMBs along with the biomolecules they have bound to. Achieving a high capture efficiency, which is the ratio of captured mMBs to the total mMBs in the system, is crucial to minimize errors

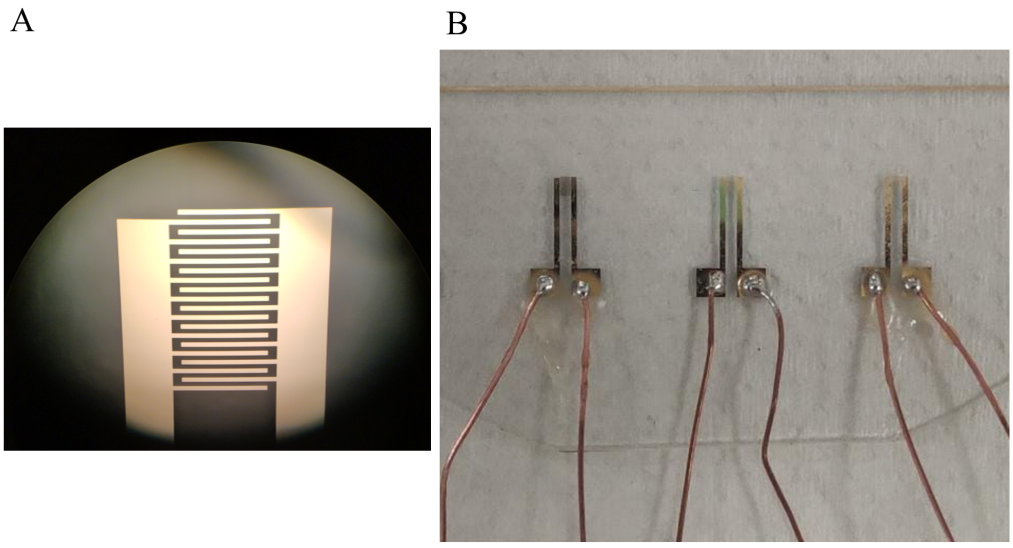


Figure 2.4: (A) Interdigitated microelectrodes under the microscope, (B) Series of electrodes on a glass wafer.

in microfluidic devices. The use of mMBs offers advantages such as easy isolation within the system using an external magnetic field, a high surface area-to-volume ratio allowing for ample binding sites, and customization to target different biomolecules [103, 104]. These characteristics make separation using mMBs a highly promising option for integration into microfluidics systems. This approach ensures reliability and versatility in its application. The aptamer is attached to surface-modified superparamagnetic microparticles that are used for bacteria detection. The superparamagnetic microparticles are synthesized step-wisely as described in the literature [105]. Briefly, the template seed particle poly(GMA) is synthesized *via* dispersion polymerization [106]. 3 mL of glycidyl methacrylate (GMA) monomer, 0.45 g polyvinylpyrrolidone K30 (PVP-K30) stabilizer, and 0.24 g $2,2'$-Azobisizobutyronitrile (AIBN) thermal initiator are dissolved in 30 mL of absolute ethanol by 5-min ultrasonication. The mixture polymerizes at 70°C overnight. The particles are then collected *via* centrifugation and washed with ethanol and distilled water to obtain poly(GMA) particles.

The seed particles are used to fabricate superparamagnetic monodisperse polymeric particles, which are about 5 µm in size *via* the multistage shape-template polymerization technique. Poly (GMA) seed latex (1.0 mL, solid content 0.3 g)

and 2.5 mL ethylbenzene (EB) are added into 50 ml deionized water containing 0.125 g sodium dodecyl sulfate (SDS) to prob-sonication 6min. The suspension is magnetically stirred at room temperature overnight for the swelling process. The monomer 1.0 g of mono-2-(methacryloyloxy) ethyl succinate (MMES), the crosslinker 5 mL of ethylene glycerol dimethacrylate (EGDMA), and the thermal initiator 0.25 g of benzoyl peroxide (BPO) are dissolved in each other. The monomer mixture is dispersed into 50 mL deionized water containing 0.125 g sodium dodecyl sulfate (SDS) to prob-sonication 6 min. This emulsion is added to the swollen seed mixture and magnetically stirred at room temperature overnight for diffusion. Then aqueous polyvinyl alcohol (PVA) solution (10 mL, 8% wt/wt) is added to the final mixture that polymerizes at 80°C in a shaking water bath at 120 rpm for 24 h. After the polymerization, the poly(MMES-co-EGDMA) particles are collected *via* centrifugation and washed with ethanol, tetrahydrofuran, and ethanol.

The polymeric particles are magnetized *via* co-precipitation of iron slats. 0.268 g of $FeCl_2{\cdot}4H_2O$ and 0.4 g $FeCl_2{\cdot}6H_2O$ are dissolved in 10 mL deionized water under nitrogen atmosphere. 1 g of poly(MMES-co-EGDMA) is dispersed in 50 mL of deionized water and placed on ice-bath. The iron salt mixture is added to the particle solution and evacuated via a vacuum pump. The brown mixture is mechanically stirred and placed in an oil bath at 85°C. 12.5 mL of $NH_4OH$ (25% wt/wt) is added to this mixture, whereby the color instantly changes to black. The mixture is mechanically stirred for one hour, collected naturally, and washed with 0.1M HCl and deionized water several times.

The magnetic-polymeric particles are used as a template to fabricate silica particles described in the literature [107]. 0.4 g of magnetic polymeric particles are dispersed in 50 mL isopropanol (Iso-PrOH), 5 mL distilled water, 0.25 g tetrabutylammonium iodide(TBAI), and 0.25 mL $NH_4OH$ (25% wt/wt) in an ultrasonic bath. This mixture is mechanically stirred for one hour. Then 1.0 mL tetraethyl orthosilicate (TEOS) and 4 mL Iso-PrOH solution are taken in a 5 mL syringe and added drop wise onto the mixture. The mixture is then mechanically stirred for 24 h at 30°C and collected by a strong natural magnet to be washed twice with Iso-PrOH and distilled water. The silica-polymer hybrid structure is

calcined up to 450°C for 6 h with 2°C heating rate.

A bio-based green route for particle surface modification is used to obtain functional groups on superparamagnetic monodisperse microparticles [108]. The mimic of mussel adhesive protein dopamine is used to obtain polydopamine (PDA) on superparamagnetic particles. Basically, 0.25 g of the magnetic particle and DOPA HCl (2 mg/mL) are dispersed in 10 mL of pH 8.5 Tris buffer. The mixture is mechanically stirred in the dark hood for 6 h. Then the particles are collected *via* a strong natural magnet and washed with deionized water several times.

### 2.4.1 Particle characterization

The morphological structure of the particles is characterized *via* scanning electron microscope (SEM, Quanta 450 SEM; Akishima, Tokyo, Japan) and Energy-dispersive X-ray spectroscopy (EDX, Quanta 450 SEM; Akishima, Tokyo, Japan). The chemical structure of the particles is determined using Fourier-transform infrared spectroscopy. The magnetic properties are analyzed by vibrating sample magnetometer (VSM-Cryogenic Limited Model: PPM system, UK).

The particles are obtained in monodisperse around 6 μm in size as seen in Figure 2.5A. The carbon, oxygen, and iron content on the surface of the particle is determined *via* EDX. The organic and inorganic hybrid content is obtained around 69.3% C, 17.4% O, 13.3% Fe as weight percentages and 81.3% C, 15.3% O, 3.3% Fe as atomic percentages. The chemical structure of the particles is analyzed with FTIR. The FTIR spectrum shows the inorganic part $Fe_2O_3$ characteristic peaks at 560 and 690 $cm^{-1}$. The strong Si-O peak can be seen at 1010 $cm^{-1}$. The organic part of the particles can be seen with a strong peak at 1720 $cm^{-1}$ as a C=O bond and C-H stretching at 2880 and 2980 $cm^{-1}$. The broad peak at 3500 $cm^{-1}$ is representing O-H functional groups of PDA coating on beads. The magnetic property of the particles is analyzed by drawing a hysteresis curve. The curve shows that the magnetic saturation value was around 10 emu/g and had superparamagnetic characteristics.

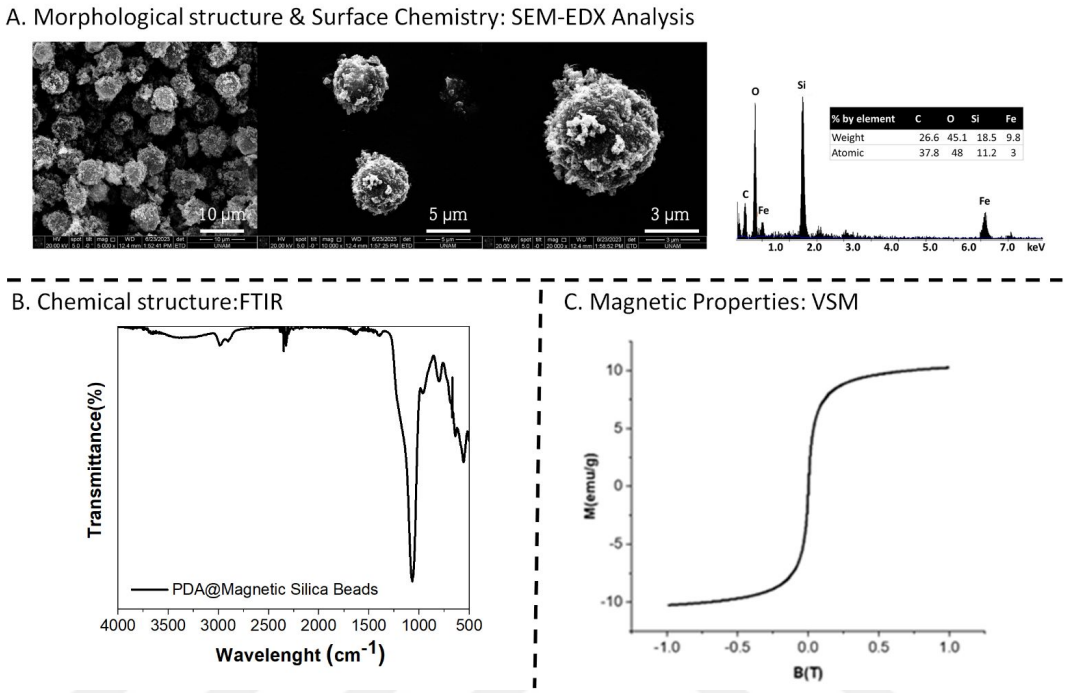


Figure 2.5: The particle characterization panel (A) morphological characteristic of the particles with EDX result, (B) chemical structure analyzed with FTIR spectrum, (C) the hysteresis curve of the particles.

### 2.4.2 Aptamer binding to particles

Aptamers, which are synthetic nucleic acid molecules created through in vitro selection methods, possess remarkable affinity and specificity for binding to specific molecular targets [109]. Various techniques are employed to immobilize aptamers onto mMBs. In this study, we utilize a specific approach that involves introducing amine groups at one end of the aptamer. This modification enables the attachment of the aptamer to carboxylated mMBs through EDC/NHS coupling. By employing this method, we achieve highly oriented immobilization of aptamers, as only the terminal amine group participates in the coupling process. To prepare the aptamer bonded mMBs, 12.9 mg/µL of the mMBs is diluted in 250 µL of PBS buffer solution. Then 100mM of NSH and EDAC are added to the solution to produce the mMBs-protein complex overnight at room temperature. Then, the purchased aptamers are added to the mixture and provided aptamer bonded MBs after four hours of waiting.

# Chapter 3

# Experimentation

The experimental setup comprises a syringe pump, a power supplier to set the voltage and the rotating speed of the motor, a magnetic platform, and a microscope. The experiments are conducted in two main parts. In the first part, using the 3D printer, we design a setup to simultaneously view mMBs loaded in the microfluidic chip under the microscope and adjust the minimum and maximum values for the flow rate to distribute the mMBs inside the microfluidic chip, and prevent them from being washed away. To achieve this, the experiments are conducted three times, noting the flow rate corresponding to changes in voltage. A schematic view and the setups used in these experiments are depicted in Figures 3.1A and 3.1B. To minimize the impact of vibration and observe the motion of particles, especially when higher voltages are involved, a separate box is designed to hold the motor casing under the microscope, as shown in Figure 3.1C. The microfluidic chip with the loaded mMBs is depicted in Figure 3.2.

The second part of the experiments involves removing the microscope and instead placing the chip loaded with magnetic particles on a different 3D-printed platform. The schematic and disassembled views of the platform are presented in Figures 3.3A and 3.3B. This modification allows for easier collection of samples from the outlet, simplifying the overall process. Figures 3.4A and 3.4B illustrate the setup used for bacteria isolation from phosphate-buffered saline (PBS) buffer

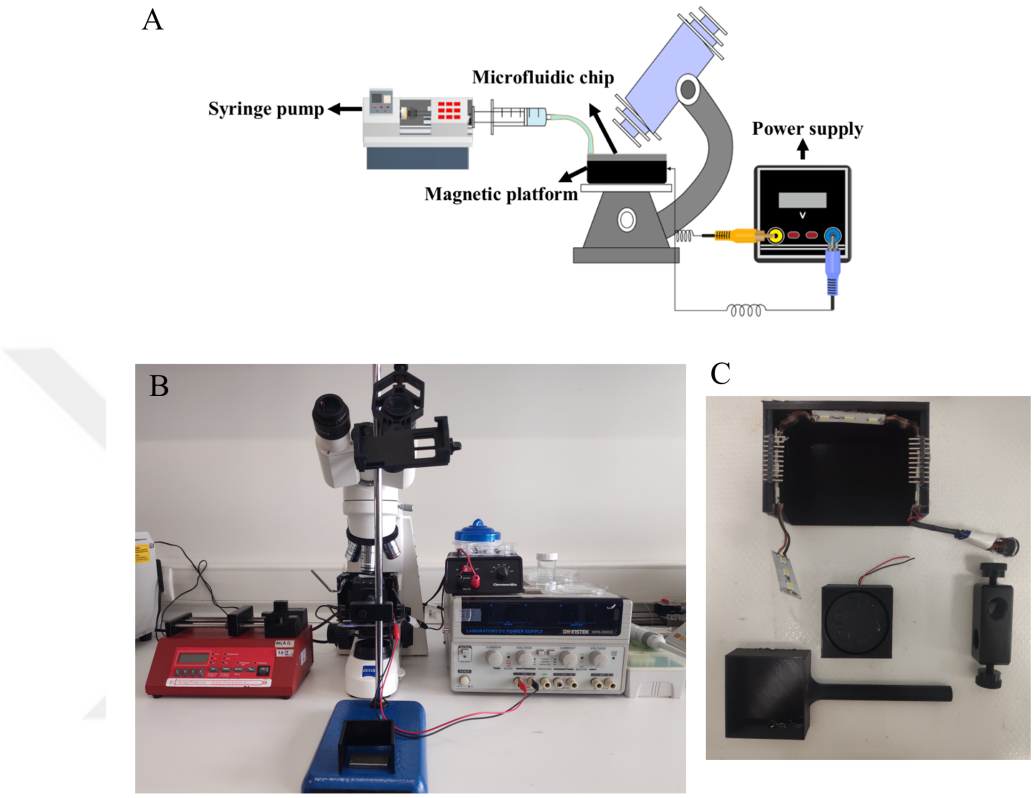


Figure 3.1: (A) Schematic view of the experimental setup, (B) experimental setup for adjusting the flow rates and voltages, (C) motor casing holder.

and blood samples.

## 3.1 Separation of bacteria with mMBs

Separating bacteria from complex mixtures presents a significant challenge. In this particular context, the utilization of mMBs that have been modified with specific ligands enables the effective isolation of the desired bacteria through the application of powerful magnets. The utilization of mMBs-based sample pre-treatment not only enables the isolation of target bacteria but also eliminates the need for time-consuming procedures such as centrifugation, filtration, and solid-phase extraction [110].

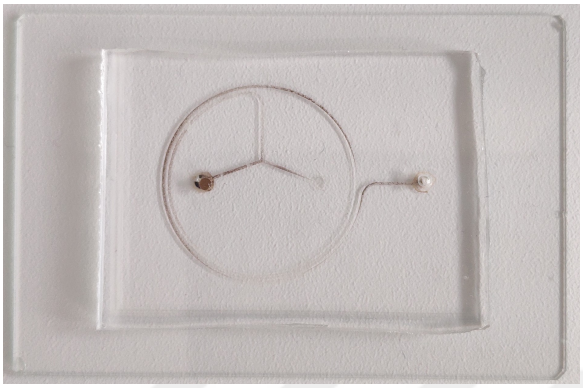

Figure 3.2: Microfluidic chip with loaded mMBs.

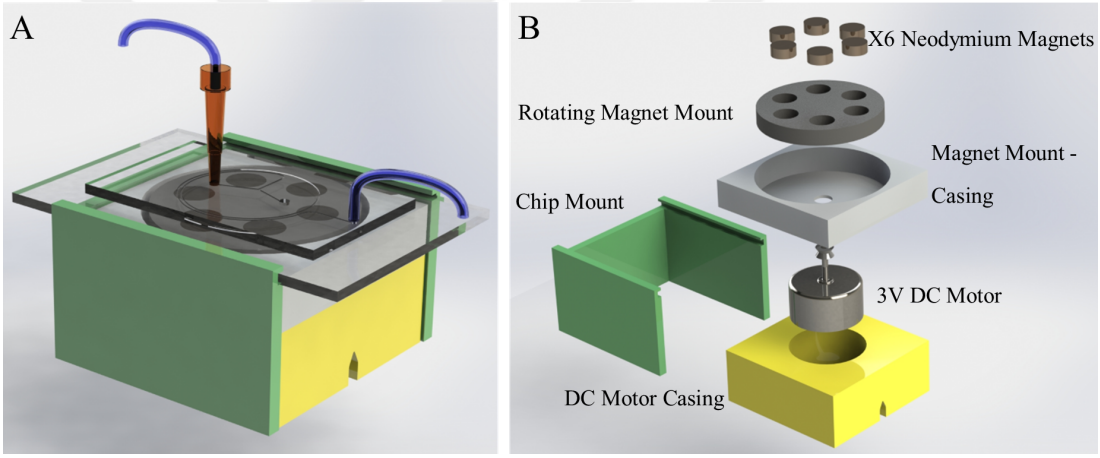


Figure 3.3: (A) Schematic view of the experimental setup, (B) disassembled view of the magnetic unit.

### 3.1.1 Batch bacterial isolation

Batch bacterial isolation with mMBs using Eppendorf tubes is a common technique used in molecular biology and microbiology labs to purify and concentrate bacterial cells from a complex sample. For batch bacteria isolation, first, 1.5 mL of bacterial culture is transferred to an Eppendorf tube and centrifuged in 5000× g for 5 minutes to pellet the bacterial cells. Next, the supernatant and resuspend of the bacterial pellet are removed in 1.0 mL of PBS buffer solution. After that, 0.1 grams of synthesized mMBs are added to the bacterial suspension and mix them, followed by incubation for 10-15 minutes at room temperature with gentle shaking. Then the Eppendorf tube is placed in a magnetic rack for 1-2 minutes

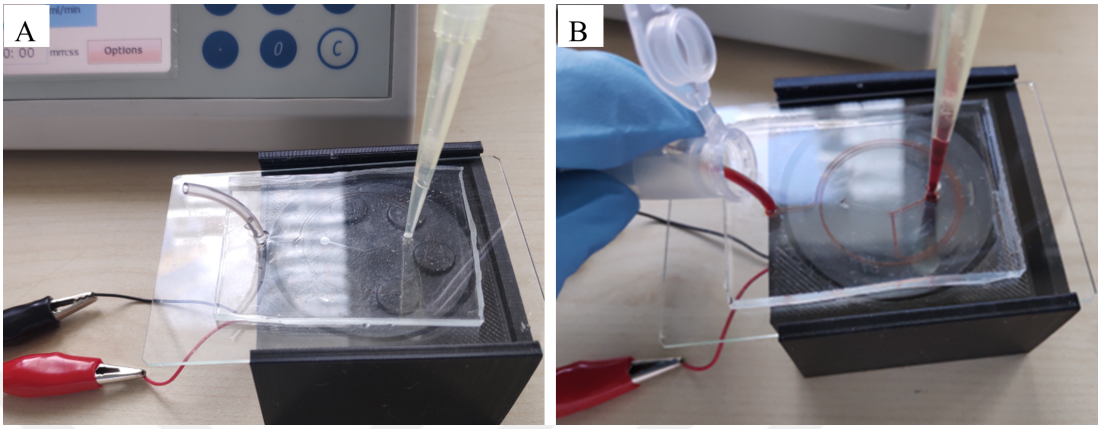


Figure 3.4: Magnetic platform for bacteria isolation: (A) PBS buffer and (B) blood samples.

to allow the mMBs to separate the bacterial cells from the solution. The supernatant is removed, and 1.0 mL of wash buffer is added to the Eppendorf tube containing the bead-bound bacteria. After resuspending the mMBs, the tube is again placed in a magnetic rack. Afterward, we remove the supernatant and wash the mMBs with 1.0 mL of 70% ethanol. After the final wash, the Eppendorf tube is removed from the magnetic separation rack, and an appropriate volume of elution buffer is poured into the tube to resuspend the bead-bound bacteria. Finally, the purified bacterial sample is transferred to a new, sterile Eppendorf tube for further analysis.

### 3.1.2 Microfluidic bacterial isolation

Magnetic particles coated with specific ligands can be utilized in microfluidic systems to capture bacteria of selective interest. These mMBs can be manipulated and concentrated by applying external magnetic fields, enabling efficient separation and isolation of the target bacteria. The experiment for microfluidic bacteria isolation is conducted at three different inlet flow rates of 30, 45, and 60 µL/min, and the device's voltage is set to control the rotational speed of the magnetic platform. For microfluidic bacteria isolation, initially, we load 0.1 mg

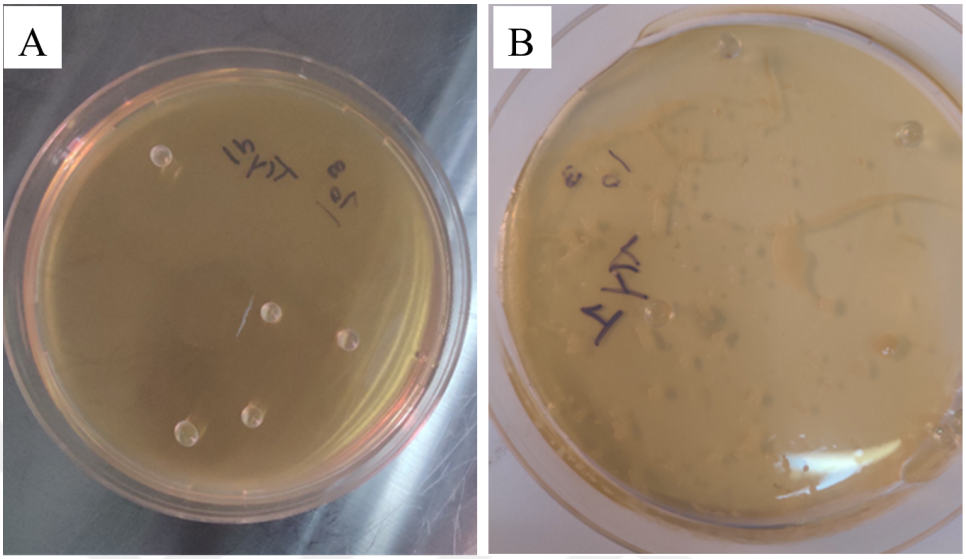


Figure 3.5: Bacteria culturing for colony counting: (A) before incubation and (B) after incubation.

of aptamer-bonded mMBs inside a clean microfluidic chip using the strong magnet and place it on top of the rotating magnetic platform presented in Figure 3.4. Using the syringe pump, the 60 μL of bacteria is taken on the pipette's tip. Afterward, the 200 μL of bacteria and PBS buffer solution is injected into the chips to eliminate the effect of the dead volume and collect the outlet into the Eppendorf tube. Also, the mMBs are washed and collected in another Eppendorf tube. The experiments are repeated three times for seven different concentrations of the bacteria (from $1 \times 10^1$ to $1 \times 10^7$ CFU/mL) plus one set of only PBS buffer to eliminate the effects of background noise or any potential interference caused by the buffer solution itself. To analyze the specific selectivity of the aptamer, we try experiments for controlling bacteria (*S. aureus*) at two different bacteria concentrations of $1 \times 10^4$ and $1 \times 10^7$ CFU/mL three times. Moreover, the experiments are repeated for bacteria inside the blood at one of the flow rates since blood reflects the natural environment for bloodstream infections. Blood cultures offer higher sensitivity compared to isolating bacteria in PBS alone, enabling the detection of low levels of bacteria in the bloodstream.

## 3.2 Assessment of viable bacterial colonies

Conventional plate counting is used to validate the bacterial capture efficiency of the mMBs. To prepare culturing medium, 5 g of Agar and 6 g of brain heart infusion are measured and solved in 200 mL of deionized (DI) water. The mixture is autoclaved for one and a half an hour before bacteria culturing. For $1 \times 10^1$ to $1 \times 10^3$ CFU/mL of bacteria, 100 µL of mMBs-bacteria complexes which are collected during washing steps after bacteria− mMBs interaction, are poured on the culturing environment and applied to cover the surface of the medium. However, higher bacteria concentrations are serially diluted in consecutive order to reach $1 \times 10^3$ CFU/mL before culturing. The bacterial colony enumerations are carried out after incubating the plates at 37°C for 18-24 hours to assess the number of viable cells in CFU/mL. Figure 3.5 presents the plates before and after incubation at 37°C. The efficiency of bacterial capture ($\eta$) is calculated according to the following Equation 3.1:

$$\eta[\%] = (C_c/C_t) \times 100 \tag{3.1}$$

$C_t$ represents the bacteria concentration [CFU/mL] in the sample, while $C_c$ refers to the bacteria concentration computed as captured bacteria level.

## 3.3 Electrochemical detection

In the past three years, interdigitated electrodes (IDEs) have emerged as the preferred choice for bacterial sensing. The primary reason for their popularity is their combination of desirable features, including minimal ohmic drop, rapid reaction kinetics, a high signal-to-noise ratio, and a compact physical footprint. These characteristics make IDEs the optimal transducers for various biosensors based on electrochemical impedance spectroscopy (EIS). By leveraging IDEs, it becomes possible to make sensitive measurements of alterations in electrochemical impedance that arise from biological reactions taking place on their surface [111]. The schematic view of the experimental procedure is presented in Figure 3.6,

Figure 3.6: Mechanism of electrochemical impedance spectroscopy (EIS) detection.

### 3.3.1 Immobilization of aptamer

Before modifying the microelectrode with aptamers for capturing the target bacteria, a series of cleaning steps are performed. Initially, the Piranha solution is dropped on the electrodes. Afterward, the microelectrode is rinsed with deionized water and dried using a nitrogen flow in order to effectively cleanse the microelectrode. Next, we introduce a thiol group (-SH) into an aptamer and mix the thiol-modified aptamer with the buffer solution in a microcentrifuge tube. Then we incubate the aptamer solution with the microelectrodes chip overnight at room temperature. After incubation, the washed microelectrodes chip is gently rinsed with the buffer solution to remove any unbound aptamer. Then the chip is immersed in a blocking agent solution (1% BSA in buffer) for around 1 hour at room temperature. This prevents non-specific binding and minimizes background signal by blocking the remaining reactive sites on the surface of the microelectrode. The chip is thoroughly washed with the buffer solution to remove any excess blocking agent. *S. pneumoniae* solutions with varying cell concentrations ($1 \times 10^1$ to $1 \times 10^7$) are dropped on the sensor surfaces 3 times. Subsequently, the sensors are placed in a 37°C environment until the liquid solution evaporated. The sensors undergo a thorough washing process to eliminate any proteins and cells that might have adhered non-specifically. They are washed with PBS containing 0.05% Tween and then rinsed multiple times with deionized water. This process is repeated for *E.coli* to validate the selectivity of the aptamers.

### 3.3.2 EIS measurements

EIS (Electrochemical Impedance Spectroscopy) measurements are carried out using an IM-6 impedance analyzer along with the IM-6/THALES software. The microelectrode is placed in a 4 mL solution of 0.01 M PBS with a pH of 7.4. The solution also contains 10 mM of [Fe(CN)6]3-/4- in a 1:1 ratio. In the setup, one of the microband array electrodes is linked to the test and sense probes, while the other is connected to the reference and counter electrodes on the IM-6 impedance analyzer. Throughout the tests, an open circuit condition is maintained. The frequency range tested ranged from 1 Hz to 100 kHz, and the amplitude is set to 5 mV. A Bode diagram (impedance and phase vs. frequency) is generated to record the data. The signal that denotes the immune reaction between the immobilized aptamers and bacteria is determined by comparing the electron-transfer resistance before and after cell binding. The SIM program is used to simulate the process, automatically selecting several data points from each measured spectrum. These data points are then used as input to create a fitting spectrum using an equivalent circuit.

# Chapter 4

# Results and Discussion

## 4.1 Effect of flow rate

Table 4.1 presents the findings from the initial phase of experiments, highlighting a notable trend between voltage and the required inlet volumetric flow rates for retaining 0.1 mg mMBs within the channel. As the voltage increases, there is a corresponding increase in the necessary flow rates. For instance, at 0.6 V, the magnetic motors initiate rotation, allowing for flow rates ranging from approximately 25 μL/min to 36 μL/min at different rotational speeds. However, it should be noted that higher voltages, which result in higher rotational speeds, induce vibrations in the experimental setups, making it challenging to observe particle motion under the microscope. Therefore, the maximum voltage suitable for capturing motion is determined to be 2.2 V. At this voltage, the flow rate can be increased to approximately 65 μL/min, providing a higher throughput while still maintaining visibility of particle motion.

Table 4.1: Voltage values and corresponding min. and max. flow rates to retain magnetic particles within the channel.

| **Voltage** [V] | **Min. flow rate** $Q_{min}$[µL/min] | **Max. flow rate** $Q_{max}$[µL/min] |
|---|---|---|
| 0.6 | 25.7 | 36.0 |
| 1.0 | 29.3 | 38.0 |
| 1.4 | 37.7 | 48.0 |
| 1.7 | 39.3 | 52.3 |
| 2.2 | 45.0 | 65.7 |

## 4.2 Bacteria isolation

### 4.2.1 PBS samples

Figure 4.1 compares the efficiency of the developed microfluidic platform and batch *S. pneumoniae* separation from the PBS buffer solution at different concentrations from $1 \times 10^1$ to $1 \times 10^7$ CFU/mL. Microfluidic bacteria isolation seems to work with higher efficiency for denser bacterial suspensions in comparison to bacterial isolation in the tube due to the increment of the area of the interaction between the bacteria solution and mMBs. In addition to the advantages mentioned, microfluidic systems offer several other benefits over batch methods. These include the potential for protocol automation, precise control of sample volumes, flow rate regulation, and the ability to conduct experiments under strictly reproducible conditions. The varied inlet volumetric flow outcomes indicate that microfluidic channels exhibit superior capture efficiency compared to batch bacteria isolation when dealing with more concentrated bacterial solutions. Additionally, higher flow rates correlated with increased capture efficiency for bacteria concentrations exceeding $1 \times 10^3$ CFU/mL. The peak efficiency, reaching approximately 83%, is attained at a flow rate of 60 µL/min for a bacteria concentration of $1 \times 10^4$ CFU/mL. When handling bacteria concentrations that are less dense (below $1 \times 10^4$ CFU/mL), microfluidic channels with a flow rate of 30 µL/min exhibit better performance, very close to the batch isolation except

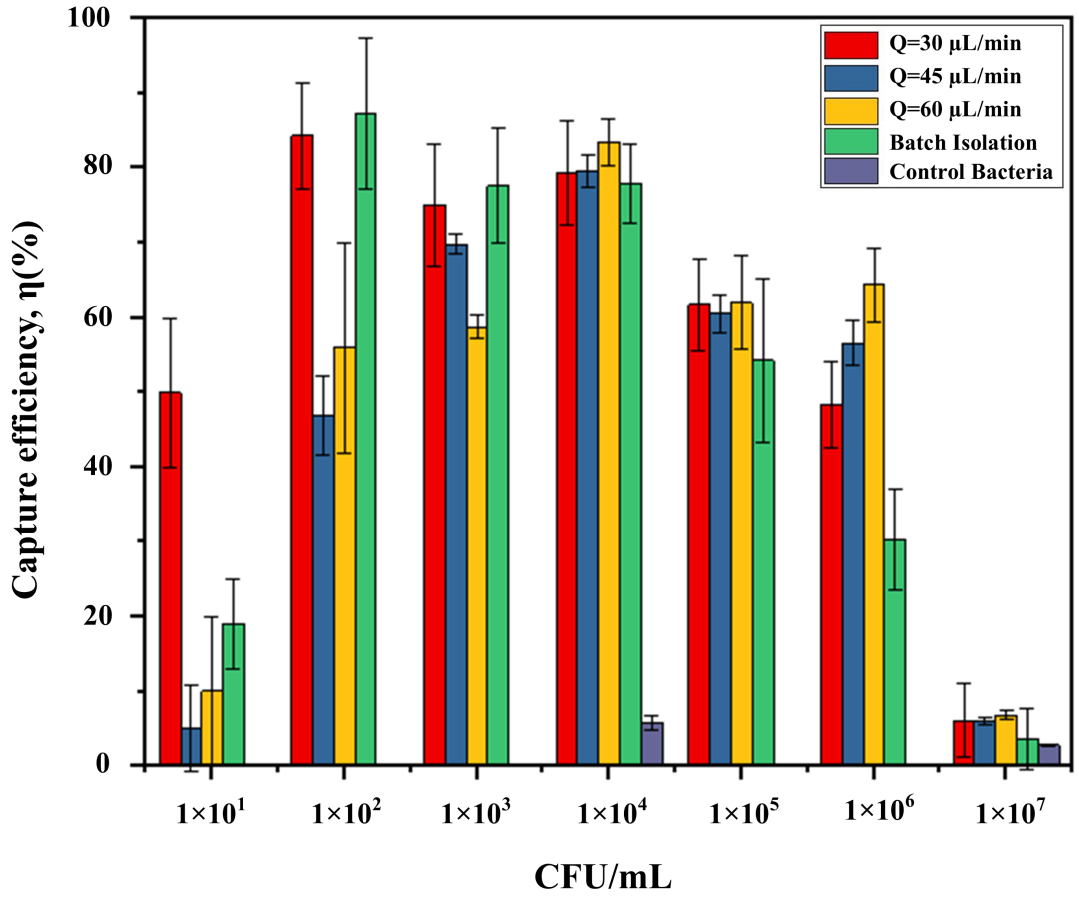


Figure 4.1: Experimental Results for bacteria isolation from PBS buffer.

for $1 \times 10^1$ CFU/mL where microfluidic channels outperform batch isolation by almost 2.5 times, achieving a capture efficiency of 50%. The reason is that for low concentrations of bacteria at low flow rates, the bacteria have more time to interact with mMBs, thereby increasing the likelihood of binding with them.

The graph also includes the results for *S. aureus*, which serves as a control bacterium to demonstrate the specificity of our selected aptamers in capturing *S. pneumoniae* . By comparing the capture efficiency of *S. aureus* to that of *S. pneumoniae*, we can validate the selectivity of our devices. At two different concentrations, namely $1 \times 10^4$ and $1 \times 10^7$, the capture efficiency of the control bacteria, *S. aureus*, is observed to be approximately 6% and 3%, respectively.

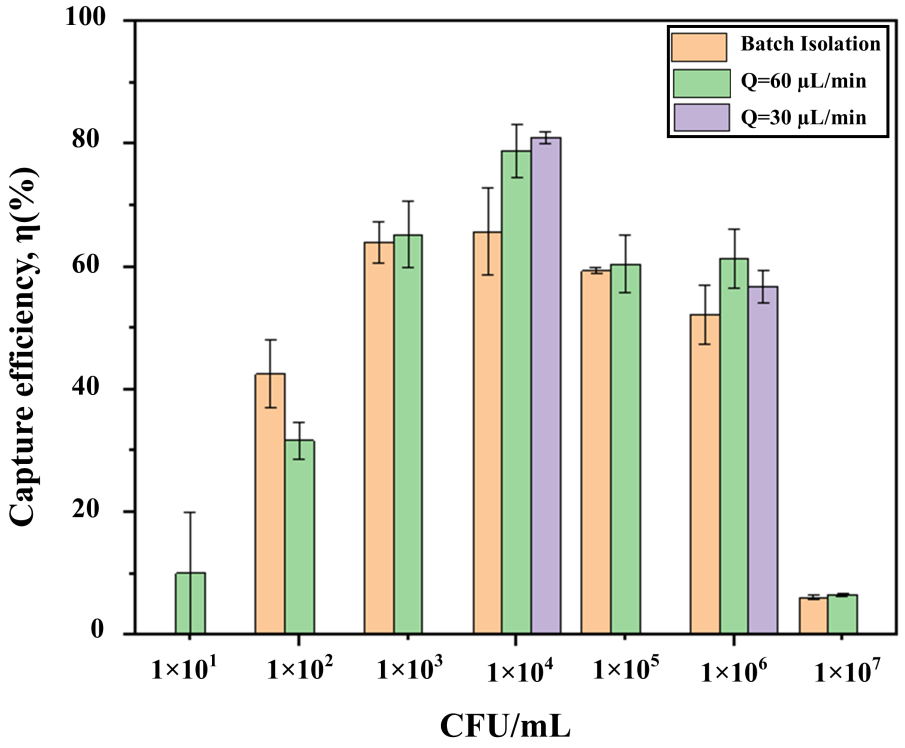


Figure 4.2: Blood bacteria isolation results.

### 4.2.2 Blood samples

This study conducted a series of experiments to isolate *S. pneumoniae* from blood samples. The outcomes of these experiments are illustrated in Figure 4.2, where different bacterial concentrations were tested at two flow rates of 30 and 60 µL/min, alongside batch isolation. Notably, the results for the lower flow rate (30 µL/min) are only available for bacterial concentrations of $1 \times 10^4$ and $1 \times 10^6$ CFU/mL.The findings demonstrate that microfluidic isolation generally outperforms batch isolation in terms of capture efficiency, particularly for denser bacterial concentrations. At a concentration of $1 \times 10^4$ CFU/mL and a flow rate of 30 µL/min, the capture efficiency is nearly 15% higher than that achieved through batch isolation, reaching a maximum capture efficiency of 80%. Moreover, it is observed that higher flow rates result in better capture efficiency, particularly for samples with denser bacterial populations.

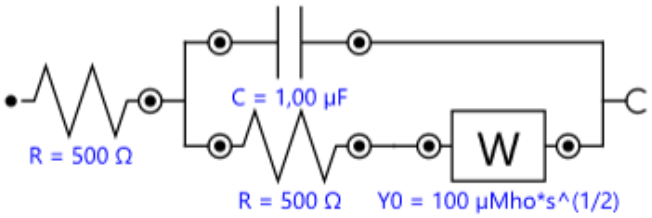


Figure 4.3: Circuit used for the calculations.

## 4.3 Electrochemical detection

The immunosensor operates based on the transduction principle and involves measuring electrochemical Faradaic impedance while using $[Fe(CN)_6]^3 - /4-$ as a redox probe. The process begins by immersing a bare microelectrode into an electrolyte solution containing the redox couple. Applying a small-amplitude ac potential (5 mV) to the electrode causes the redox couple to undergo oxidation and reduction, resulting in the transfer of electrons between two sets of array electrodes.

Upon immobilizing antibodies onto the electrode surface, they create a layer that obstructs electron transfer between the electrodes, leading to an increase in electron-transfer resistance. When bacterial cells attach to the electrode surface, the formation of aptamer-bacteria complexes adds another barrier, impeding the electrochemical process further. As a consequence, the redox probe's access to the electrode surface is restricted, resulting in a greater increase in electron-transfer resistance. The extent of this increase is directly linked to the number of bacterial cells captured by the immobilized aptamers. The immunosensor system can be represented by an equivalent circuit, as shown in Figure 4.3. The circuit can be employed to effectively simulate the electrochemical impedance spectra data, aiding in the comprehension of the immunosensor system's behavior. By incorporating elements from the general electronic equivalent model of an electrochemical cell and considering the specific features of the interdigitated microelectrode, a suggested equivalent circuit (refer to Figure 4.3) encompasses

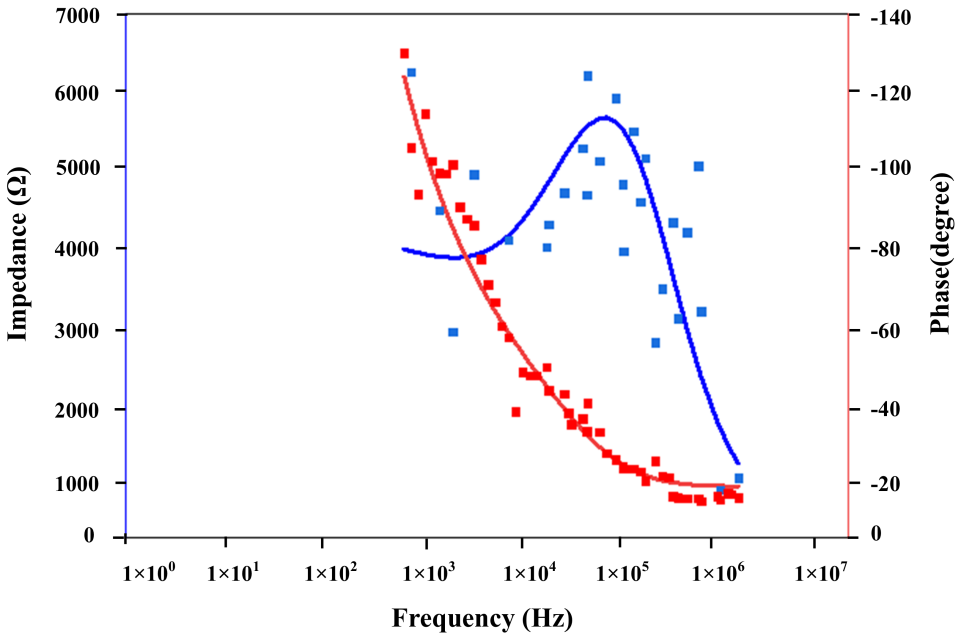


Figure 4.4: Bode diagram of the electrochemical impedance spectra of the microelectrode immunosensor, along with the corresponding fitted spectra (Square markers: measurement data, Solid line: fitting data)

crucial components essential for interpreting impedance measurements within this system.

The equivalent circuit includes the ohmic resistance of 500 Ω for the electrolyte between two electrodes and the double-layer capacitance of 1.00μF. Additionally, there is the electron-transfer resistance of 500 Ω and the Warburg impedance ($Y_0$) of 100μMho×$s^{1/2}$ surrounding each electrode. The overall current passing through the electrode surface arises from the combination of two components: the Faradaic current ($i_f$) and the double-layer current ($i_c$). A branch circuit is utilized to represent this in the equivalent circuit, consisting of the Warburg impedance in series with the electron-transfer resistance, both of which are connected in parallel with the double-layer capacitance. The two elements, namely the electrolyte resistance and $Y_o$, represent the characteristics of the bulk solution and the diffusion of the redox probe, and they are not influenced by the reactions taking place at the electrode surface. Conversely, the other two elements, capacitance and electron-transfer resistance, depend on the dielectric and insulating properties at the interface between the electrode and the electrolyte [112].

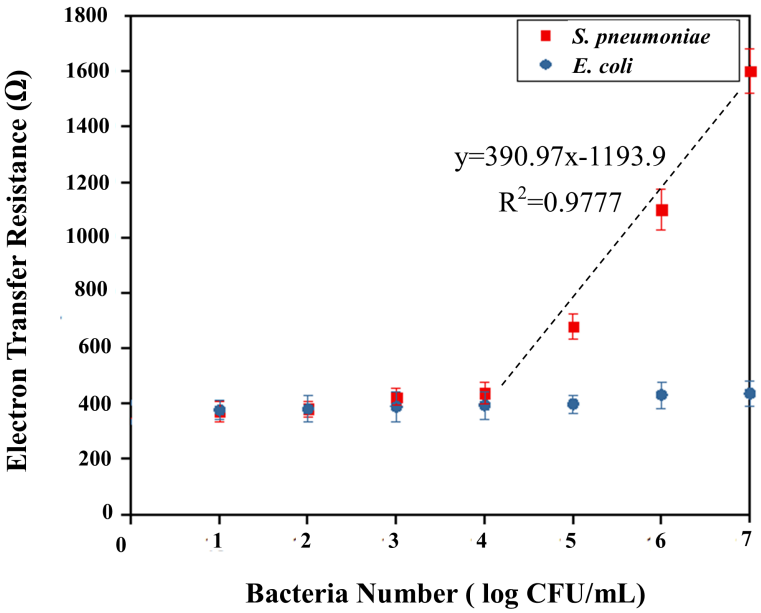


Figure 4.5: Correlation between the logarithmic value of the concentration of two types of bacteria and the electron-transfer resistance.

The Bode diagram impedance spectra of the bare interdigitated electrode are shown in Figure 4.4, represented by a solid line. The measurements are taken in a PBS buffer containing 10 mM $[Fe(CN)_6]^3 - /4-$ (1:1). This type of Bode plot is commonly observed in systems where polarization arises from a combination of diffusion and kinetic processes. To confirm the validity of the proposed equivalent circuit, the software automatically selects 50 data points from the measured impedance spectrum. These points are then used as input to the equivalent circuit, resulting in a fitting impedance spectrum shown as a solid line in Figure 4.4. The close correspondence observed between the measured data and the fitting spectra demonstrates that the proposed equivalent circuit provides a useful model for understanding the behavior of the microelectrode.

A linear relationship $y = 390.97x - 1193.7$ ($R^2 = 0.9777$) is found between the electron-transfer resistance and the logarithmic value of the *S. pneumoniae* concentrations, within the range of bacterial concentrations above $1 \times 10^4$ CFU/mL. In Figure 4.5, it is demonstrated that by using the electron-transfer resistance of the aptamer-immobilized on microelectrode as the signal threshold, the detection limit of this immunosensor is $1 \times 10^4$ CFU/mL. The aptamer-immobilized on

microelectrode is also tried for bacteria counting of *E.coli* to test the biosensors' specific selectivity. It can be seen that by increasing the bacterial concentration for *E.coli*, the electron transfer constant resistance stays constant around 400 Ω, which shows that *E.coli* cannot bind with the selected aptamers. The microelectrode represents an effective method for miniaturizing biosensors. This approach allows for the reduction of the detector device or sample volume while preserving its selectivity and sensitivity. By leveraging the biosensors utilizing microelectrodes, integration with microfluidic or micro detectors becomes possible, enabling their application in various biomedical and biotechnological fields.

# Chapter 5

# Conclusion and Future work

In this study, we revised the patented magnetic platform from our research group to efficiently isolate the *S. pneumonia* from PBS buffer solution and blood samples, followed by electrochemical detection. Firstly, the range of the inlet flow rate is determined according to the velocity of rotating magnets to retain the mMBs inside the spiral channel. Next, seven distinct concentrations of the bacteria are injected at different flow rates of 30,45, and 60 μL/min into the channel, having 0.1 mg of the aptamer-modified mMBs, and outlet samples are collected. With the same amount of mMBs, the experiments are repeated for batch bacterial isolation in an Eppendorf tube. To assess the selectivity of the aptamers, control experiments are also conducted using two different concentrations of non-target bacteria. In addition, the experiments are carried out to demonstrate the capability of the system to capture bacteria from complex biological blood samples. The plate counting method are used to evaluate the capture efficiency of the system. Microfluidic isolation reveals increased capture efficiency when dealing with higher concentrations of bacteria. The device exhibited an impressive 83% efficiency in isolating bacteria at a concentration of $1 \times 10^4$ CFU/mL, using 60 μL of loaded bacteria, all accomplished in about one minute. Furthermore, EIS measurements are also performed using the fabricated gold electrodes with immobilized aptamers on the surface. After evaluating the functionality of the system with Bode diagram, the electron transfer resistance is quantified for

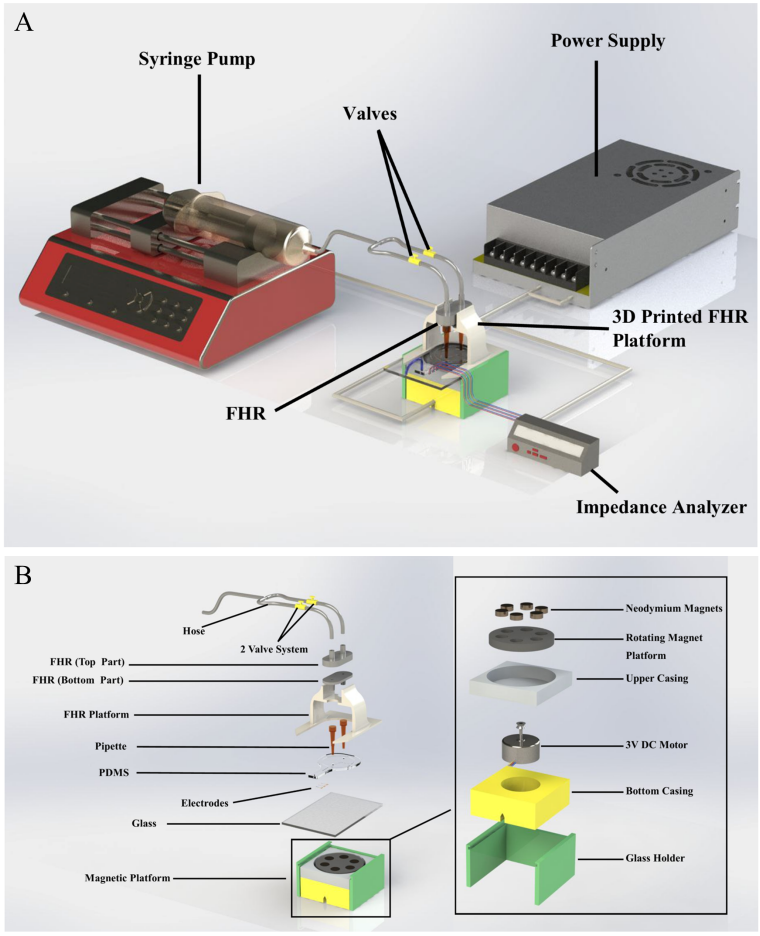


Figure 5.1: Next-generation design of an integrated device for isolation and detection.

*S. pneumoniae*, and the limit of detection is determined to be above $10 \times 10^3$ CFU/mL. To assess the biosensor's selectivity, *E. coli* was introduced onto the electrodes, and the results reveal no significant change in the resistance.

Table 5.1 presents a comparison of our results with those of other selected studies regarding the isolation and detection of bacteria. Studies with processing times exceeding one hour have been excluded. Our method represents a significant advancement compared to previous reports. One key advantage is its capability to process smaller sample amounts due to the compact dimensions of our system. Using aptamer-bonded mMBs, we can efficiently isolate 60µL of the bacteria sample within just one minute. Furthermore, our method achieves a

notable improvement in the detection limit for *S. pneumoniae* compared to conventional ELISA and magnetic microfluidics ELISA. Specifically, the detection limit is enhanced to $1 \times 10^4$ CFU/mL. This improvement is of utmost importance in increasing sensitivity in bacterial detection, thereby enabling accurate identification even at lower concentrations.

Although the isolation and detection units are fabricated and tested separately, the integration of both units is straightforward, and actually, once the electrodes are deposited on the substrate, the same mold used for the fabrication of the spiral channel can also be utilized for the fabrication of the integrated device. One of the potential limitations of this study is sample loss while loading the bacterial sample. This can be improved by using our group's patented FHR technology. In light of the findings of this thesis work, a CAD design of the next-generation integrated microfluidic platform is performed and demonstrated in Figure 5.1. For this next-generation design, the channel dimensions may be further modified, and the corresponding sample flow rates can be optimized to achieve better capture efficiency. A smaller channel size is expected to enhance capture efficiency by increasing the probability of interaction between bacteria and mMBs. However, it also results in a reduced flow rate and a lower number of analyzed mMBs-*S. pneumonia* complexes while increasing the likelihood of channel clogging.

Table 5.1: Comparing the results for bacteria detection.

| | **Bacteria type** | **Process time** | **Sample volume** | **Strategy** | **Detection range** |
|---|---|---|---|---|---|
| Conventional ELISA* [3] | *S. pneumoniae* | 30 mins | NG | Antibody | $\sim 10^6 - 10^9$ |
| MMF-ELISA* [3] | *S. pneumoniae* | 12 mins | NG | Antibody | $\sim 10^5 - 10^7$ |
| PCR+ Electrophoresis* [49] | *E.coli* | 50 mins | 2.5 mL | Antibody | LOC=10 |
| MSNT+Impedimetric [96] | *S. typhimurium* | 30 mins | NG | Antibody | $10^5 - 10^7$ |
| Magnetic-assisted+Fluorescence * [85] | *E.coli* | 1 h | 1 μL | Antibody | $5 - 5000$ |
| Virtual Net+ATP luminescence [93] | *E.coli* | 15 mins | 10 mL | Antibody | LOC=$10^2$ |
| AbMNCs+ATP luminescence* [87] | *Salmonella* | 3 mins | 10 mL | Antibody | LOC=10 |
| This Study | *S. pneumoniae* | $\sim$ 1 min | $\sim$ 10 μL | Aptamer | $\sim 10^4 - 10^7$ |

* Microfluidic

# Bibliography


[1] M. E. Pavan, E. E. Pavan, S. P. Glaeser, C. Etchebehere, P. Kämpfer, M. J. Pettinari, and N. I. López, "Proposal for a new classification of a deep branching bacterial phylogenetic lineage: transfer of coprothermobacter proteolyticus and coprothermobacter platensis to coprothermobacteraceae fam. nov., within coprothermobacterales ord. nov., coprothermobacteria classis nov. and coprothermobacterota phyl. nov. and emended description of the family thermodesulfobiaceae," *Int. J. Syst. Evol. Microbiol.*, vol. 68, no. 5, pp. 1627–1632, 2018.

[2] J. P. Lynch and G. G. Zhanel, "*Streptococcus pneumoniae*: epidemiology, risk factors, and strategies for prevention," in *Seminars in respiratory and critical care medicine*, vol. 30, pp. 189–209, © Thieme Medical Publishers, 2009.

[3] C.-C. Weng, C.-Y. Chao, S.-T. Wu, P.-H. Tsou, W.-T. Chen, B.-R. Li, and Y.-K. Li, "Integration of ni/nio nanoparticles and a microfluidic elisa chip to generate a sensing platform for *Streptococcus pneumoniae* detection," *RSC Adv.*, vol. 11, no. 46, pp. 28551–28556, 2021.

[4] A. Kopenhagen, I. Ramming, B. Camp, S. Hammerschmidt, M. Fulde, M. Müsken, M. Steinert, and S. Bergmann, "*Streptococcus pneumoniae* affects endothelial cell migration in microfluidic circulation," *Front Microbiol*, vol. 13, p. 852036, 2022.

[5] Y. Zhang, D. J. Isaacman, R. M. Wadowsky, J. Rydquist-White, J. C. Post, and G. D. Ehrlich, "Detection of *Streptococcus pneumoniae* in whole blood by pcr," *J. Clin. Microbiol.*, vol. 33, no. 3, pp. 596–601, 1995.

[6] J. C. McDonald, D. C. Duffy, J. R. Anderson, D. T. Chiu, H. Wu, O. J. Schueller, and G. M. Whitesides, "Fabrication of microfluidic systems in poly (dimethylsiloxane)," *J. Electrophor.*, vol. 21, no. 1, pp. 27–40, 2000.

[7] B. Çetin, M. B. Özer, and M. E. Solmaz, "Microfluidic bio-particle manipulation for biotechnology," *Biochem. Eng. J.*, vol. 92, pp. 63–82, 2014.

[8] S. C. Terry, J. H. Jerman, and J. B. Angell, "A gas chromatographic air analyzer fabricated on a silicon wafer," *IEEE Trans. Electron Devices*, vol. 26, no. 12, pp. 1880–1886, 1979.

[9] W. Zhou, J. Le, Y. Chen, Y. Cai, Z. Hong, and Y. Chai, "Recent advances in microfluidic devices for bacteria and fungus research," *TrAC, Trends Anal. Chem.*, vol. 112, pp. 175–195, 2019.

[10] F. Bonyadi, M. Kavruk, S. Ucak, B. Çetin, G. Bayramoglu, A. D. Dursun, Y. Arica, and V. C. Ozalp, "Real-time biosensing bacteria and virus with quartz crystal microbalance: Recent advances, opportunities, and challenges," *Critical Reviews in Analytical Chemistry*, pp. 1–12, 05 2023.

[11] J. Khandurina and A. Guttman, "Bioanalysis in microfluidic devices," *J. Chromatogr. A*, vol. 943, no. 2, pp. 159–183, 2002.

[12] B. Çetin and D. Li, "Continuous particle separation based on electrical properties using alternating current dielectrophoresis," *Electrophoresis*, vol. 30, pp. 3124–3133, 2023/08/01 2009.

[13] Y. Kang, B. Çetin, Z. Wu, and D. Li, "Continuous particle separation with localized ac-dielectrophoresis using embedded electrodes and an insulating hurdle," *Electrochimica Acta*, vol. 54, no. 6, pp. 1715–1720, 2009.

[14] B. Çetin and D. Li, "Dielectrophoresis in microfluidics technology," *Electrophoresis*, vol. 32, pp. 2410–2427, 2023/08/01 2011.

[15] S. Zeinali, B. Çetin, S. N. B. Oliaei, and Y. Karpat, "Fabrication of continuous flow microfluidics device with 3d electrode structures for high throughput dep applications using mechanical machining," *Electrophoresis*, vol. 36, pp. 1432–1442, 2023/08/01 2015.

[16] B. Çetin, M. B. Özer, E. Çağatay, and S. Büyükkoçak, "An integrated acoustic and dielectrophoretic particle manipulation in a microfluidic device for particle wash and separation fabricated by mechanical machining," *Biomicrofluidics*, vol. 10, no. 1, p. 014112, 2016.

[17] H. N. Açıkgöz, A. Karaman, M. A. Şahin, Ö. R. Çaylan, G. C. Büke, E. Yıldırım, İ. C. Eroğlu, A. E. Erson-Bensan, B. Çetin, and M. B. Özer, "Assessment of silicon, glass, FR4, PDMS and PMMA as a chip material for acoustic particle/cell manipulation in microfluidics," *Ultrasonics*, vol. 129, p. 106911, 2023.

[18] G. Kibar, U. Çalışkan, E. Y. Erdem, and B. Çetin, "One-pot synthesis of organic–inorganic hybrid polyhedral oligomeric silsesquioxane microparticles in a double-zone temperature controlled microfluidic reactor," *J. Polymer Sci. Part A: Polymer Chem.*, vol. 57, pp. 1396–1403, 2023/08/01 2019.

[19] M. D. Aşık, M. Kaplan, B. Çetin, and N. Sağlam, "Synthesis of iron oxide core chitosan nanoparticles in a 3d printed microfluidic device," *J. Nanoparticle Res.*, vol. 23, no. 3, p. 62, 2021.

[20] Y. Hu, A. Gopal, K. Lin, Y. Peng, E. Tasciotti, X. J. Zhang, and M. Ferrari, "Microfluidic enrichment of small proteins from complex biological mixture on nanoporous silica chip," *Biomicrofluidics*, vol. 5, no. 1, 2011.

[21] C. A. Baker and M. G. Roper, "A continuous-flow, microfluidic fraction collection device," *J. Chromatogr. A*, vol. 1217, no. 28, pp. 4743–4748, 2010.

[22] F. Hol and C. Dekker, "Zooming in to see the bigger picture: using nanofabrication to study bacteria," *Science*, vol. 346, pp. 1–11, 2014.

[23] G. Düven, B. Çetin, H. Kurtuldu, G. T. Gündüz, Ş. Tavman, and D. Kışla, "A portable microfluidic platform for rapid determination of microbial load and somatic cell count in milk," *Biomed. Microdev.*, vol. 21, no. 3, p. 49, 2019.

[24] K. Ren, J. Zhou, and H. Wu, "Materials for microfluidic chip fabrication," *Acc. Chem. Res.*, vol. 46, no. 11, pp. 2396–2406, 2013.

[25] A. Abou-Hassan, O. Sandre, and V. Cabuil, "Microfluidics in inorganic chemistry," *Angew. Chem. Int. Ed.*, vol. 49, no. 36, pp. 6268–6286, 2010.

[26] M. Fleger, D. Siepe, and A. Neyer, "Microfabricated polymer analysis chip for optical detection," in *IEE Proceedings-Nanobiotechnology*, vol. 151, pp. 159–161, IET, 2004.

[27] D. Kim and D. J. Beebe, "Hydrogel-based reconfigurable components for microfluidic devices," *Lab Chip*, vol. 7, no. 2, pp. 193–198, 2007.

[28] N. Lopez-Ruiz, V. F. Curto, M. M. Erenas, F. Benito-Lopez, D. Diamond, A. J. Palma, and L. F. Capitan-Vallvey, "Smartphone-based simultaneous ph and nitrite colorimetric determination for paper microfluidic devices," *Anal. Chem.*, vol. 86, no. 19, pp. 9554–9562, 2014.

[29] J. C. McDonald and G. M. Whitesides, "Poly (dimethylsiloxane) as a material for fabricating microfluidic devices," *Acc. Chem. Res.*, vol. 35, no. 7, pp. 491–499, 2002.

[30] E. Gencturk, S. Mutlu, and K. O. Ulgen, "Advances in microfluidic devices made from thermoplastics used in cell biology and analyses," *Biomicrofluidics*, vol. 11, no. 5, 2017.

[31] D. J. Harrison, K. Fluri, K. Seiler, Z. Fan, C. S. Effenhauser, and A. Manz, "Micromachining a miniaturized capillary electrophoresis-based chemical analysis system on a chip," *Science*, vol. 261, no. 5123, pp. 895–897, 1993.

[32] T. Doerks, R. R. Copley, J. Schultz, C. P. Ponting, and P. Bork, "Systematic identification of novel protein domain families associated with nuclear functions," *Genome Res.*, vol. 12, no. 1, pp. 47–56, 2002.

[33] P. Hoffmann, U. Häusig, P. Schulze, and D. Belder, "Microfluidic glass chips with an integrated nanospray emitter for coupling to a mass spectrometer," *Angew. Chem. Int. Ed.*, vol. 46, no. 26, pp. 4913–4916, 2007.

[34] P. Sabounchi, A. M. Morales, P. Ponce, L. P. Lee, B. A. Simmons, and R. V. Davalos, "Sample concentration and impedance detection on a microfluidic polymer chip," *Biomed. Microdevices*, vol. 10, pp. 661–670, 2008.

[35] L. Yi, W. Xiaodong, and Y. Fan, "Microfluidic chip made of cop (cyclo-olefin polymer) and comparison to pmma (polymethylmethacrylate) microfluidic chip," *J. Mater. Process. Technol.*, vol. 208, no. 1-3, pp. 63–69, 2008.

[36] A. D. Stroock and G. M. Whitesides, "Controlling flows in microchannels with patterned surface charge and topography," *Acc. Chem. Res.*, vol. 36, no. 8, pp. 597–604, 2003.

[37] G. Aumiller, E. Chandross, W. Tomlinson, and H. Weber, "Submicrometer resolution replication of relief patterns for integrated optics," *J. Appl. Phys.*, vol. 45, no. 10, pp. 4557–4562, 1974.

[38] S. Masuda, M. Washizu, and T. Nanba, "Novel method of cell fusion in field constriction area in fluid integration circuit," *IEEE Trans. Ind. Appl.*, vol. 25, no. 4, pp. 732–737, 1989.

[39] D. C. Duffy, J. C. McDonald, O. J. Schueller, and G. M. Whitesides, "Rapid prototyping of microfluidic systems in poly (dimethylsiloxane)," *Anal. Chem.*, vol. 70, no. 23, pp. 4974–4984, 1998.

[40] R. O'Connor, X. Hao, K. Shen, K. Bashour, L. Kam, and M. Milone, "Substrate rigidity regulates human t cell activation and proliferation (52.9)," *J. Immunol.*, vol. 188, no. 1_Supplement, pp. 52–9, 2012.

[41] T. Merkel, V. Bondar, K. Nagai, B. Freeman, and I. Pinnau, "Gas sorption, diffusion, and permeation in poly (dimethylsiloxane)," *J Polym Sci B Polym Phys .*, vol. 38, no. 3, pp. 415–434, 2000.

[42] V. Liu, Y.-A. Song, and J. Han, "Capillary-valve-based fabrication of ion-selective membrane junction for electrokinetic sample preconcentration in pdms chip," *Lab Chip.*, vol. 10, no. 11, pp. 1485–1490, 2010.

[43] H. Sato, H. Matsumura, S. Keino, and S. Shoji, "An all su-8 microfluidic chip with built-in 3d fine microstructures," *J Micromech Microeng*, vol. 16, no. 11, p. 2318, 2006.

[44] Y. Zheng, W. Dai, D. Ryan, and H. Wu, "Fabrication of freestanding, microperforated membranes and their applications in microfluidics," *Biomicrofluidics*, vol. 4, no. 3, 2010.

[45] B. Çetin, A. K. Koska, and M. Erdal, "Warpage Characterization of Microchannels Fabricated by Injection Molding," *J. Micro Nano-Manuf.*, vol. 3, p. 021005, 06 2015.

[46] N. W. Choi, M. Cabodi, B. Held, J. P. Gleghorn, L. J. Bonassar, and A. D. Stroock, "Microfluidic scaffolds for tissue engineering," *Nat. Mater*, vol. 6, no. 11, pp. 908–915, 2007.

[47] G. Xing, W. Zhang, N. Li, Q. Pu, and J.-M. Lin, "Recent progress on microfluidic biosensors for rapid detection of pathogenic bacteria," *Chin Chem Lett .*, vol. 33, no. 4, pp. 1743–1751, 2022.

[48] J. Nie, Q. Gao, Y. Wang, J. Zeng, H. Zhao, Y. Sun, J. Shen, H. Ramezani, Z. Fu, Z. Liu, *et al.*, "Vessel-on-a-chip with hydrogel-based microfluidics," *Small*, vol. 14, no. 45, p. 1802368, 2018.

[49] A. T. Abafogi, J. Kim, J. Lee, M. O. Mohammed, D. van Noort, and S. Park, "3d-printed modular microfluidic device enabling preconcentrating bacteria and purifying bacterial dna in blood for improving the sensitivity of molecular diagnostics," *Sensors*, vol. 20, no. 4, p. 1202, 2020.

[50] T. Mairal, V. C. Özalp, P. Lozano Sánchez, M. Mir, I. Katakis, and C. K. O'Sullivan, "Aptamers: molecular tools for analytical applications," *Anal. Bioanal. Chem.*, vol. 390, no. 4, pp. 989–1007, 2008.

[51] C.-H. Wang, J.-J. Wu, and G.-B. Lee, "Screening of highly-specific aptamers and their applications in paper-based microfluidic chips for rapid diagnosis of multiple bacteria," *Sens. Actuators B Chem.*, vol. 284, pp. 395–402, 2019.

[52] H. Xu, X. Mao, Q. Zeng, S. Wang, A.-N. Kawde, and G. Liu, "Aptamer-functionalized gold nanoparticles as probes in a dry-reagent strip biosensor for protein analysis," *Anal. Chem.*, vol. 81, no. 2, pp. 669–675, 2009.

[53] J. Zhan, L. Wang, Y. Zhu, H. Gao, Y. Chen, J. Chen, Y. Jia, J. He, Z. Fang, Y. Zhu, *et al.*, "Temperature-controlled reversible exposure and hiding of antimicrobial peptides on an implant for killing bacteria at room temperature and improving biocompatibility in vivo," *ACS Appl. Mater. Interfaces*, vol. 10, no. 42, pp. 35830–35837, 2018.

[54] K. Yuan, Q. Mei, X. Guo, Y. Xu, D. Yang, B. J. Sánchez, B. Sheng, C. Liu, Z. Hu, G. Yu, *et al.*, "Correction: Antimicrobial peptide based magnetic recognition elements and au@ ag-go sers tags with stable internal standards: a three in one biosensor for isolation, discrimination and killing of multiple bacteria in whole blood," *Chem. Sci.*, vol. 10, no. 2, pp. 635–635, 2019.

[55] F. Mi, C. Hu, Y. Wang, L. Wang, F. Peng, P. Geng, and M. Guan, "Recent advancements in microfluidic chip biosensor detection of foodborne pathogenic bacteria: a review," *Anal. Bioanal. Chem.*, vol. 414, no. 9, pp. 2883–2902, 2022.

[56] M. Kwiatek, S. Parasion, and A. Nakonieczna, "Therapeutic bacteriophages as a rescue treatment for drug-resistant infections–an in vivo studies overview," *J. Appl. Microbiol.*, vol. 128, no. 4, pp. 985–1002, 2020.

[57] Q. Shang, Y. Su, Y. Liang, W. Lai, J. Jiang, H. Wu, and C. Zhang, "Ultrasensitive cloth-based microfluidic chemiluminescence detection of listeria monocytogenes hlya gene by hemin/g-quadruplex dnazyme and hybridization chain reaction signal amplification," *Anal. Bioanal. Chem.*, vol. 412, pp. 3787–3797, 2020.

[58] L. Zheng, G. Cai, S. Wang, M. Liao, Y. Li, and J. Lin, "A microfluidic colorimetric biosensor for rapid detection of *Escherichia coli O157: H7* using gold nanoparticle aggregation and smart phone imaging," *Biosens. Bioelectron.*, vol. 124, pp. 143–149, 2019.

[59] J. Jiang, H. Wu, Y. Su, Y. Liang, B. Shu, and C. Zhang, "Electrochemical cloth-based dna sensors (ecdss): A new class of electrochemical gene sensors," *Anal. Chem.*, vol. 92, no. 11, pp. 7708–7716, 2020.

[60] Y. Hou, W. Tang, W. Qi, X. Guo, and J. Lin, "An ultrasensitive biosensor for fast detection of *Salmonella* using 3d magnetic grid separation and urease catalysis," *Biosens. Bioelectron.*, vol. 157, p. 112160, 2020.

[61] E. Cesewski and B. N. Johnson, "Electrochemical biosensors for pathogen detection," *Biosens. Bioelectron.*, vol. 159, p. 112214, 2020.

[62] X. Tan, A. David, J. Day, H. Tang, E. R. Dixon, H. Zhu, Y.-C. Chen, M. K. Khaing Oo, A. Shikanov, and X. Fan, "Rapid mouse follicle stimulating hormone quantification and estrus cycle analysis using an automated microfluidic chemiluminescent elisa system," *ACS Sens.*, vol. 3, no. 11, pp. 2327–2334, 2018.

[63] S. Zelenin, J. Hansson, S. Ardabili, H. Ramachandraiah, H. Brismar, and A. Russom, "Microfluidic-based isolation of bacteria from whole blood for sepsis diagnostics," *Biotechnol. Lett.*, vol. 37, pp. 825–830, 2015.

[64] W.-H. Chang, C.-H. Wang, S.-Y. Yang, Y.-C. Lin, J.-J. Wu, M. S. Lee, and G.-B. Lee, "An integrated microfluidic system for rapid isolation and detection of live bacteria in periprosthetic joint infections," in *2014 IEEE 27th International Conference on Micro Electro Mechanical Systems (MEMS)*, pp. 5–8, IEEE, 2014.

[65] M. A. Faridi, H. Ramachandraiah, I. Banerjee, S. Ardabili, S. Zelenin, and A. Russom, "Elasto-inertial microfluidics for bacteria separation from whole blood for sepsis diagnostics," *J. Nanobiotechnology*, vol. 15, pp. 1–9, 2017.

[66] L. Yao, L. Zheng, G. Cai, S. Wang, L. Wang, and J. Lin, "A rapid and sensitive *Salmonella* biosensor based on viscoelastic inertial microfluidics," *Sensors*, vol. 20, no. 9, p. 2738, 2020.

[67] M. R. Condina, B. A. Dilmetz, S. R. Bazaz, J. Meneses, M. E. Warkiani, and P. Hoffmann, "Rapid separation and identification of beer spoilage bacteria by inertial microfluidics and maldi-tof mass spectrometry," *Lab Chip*, vol. 19, no. 11, pp. 1961–1970, 2019.

[68] S. Narayana Iyengar, T. Kumar, G. Mårtensson, and A. Russom, "High resolution and rapid separation of bacteria from blood using elasto-inertial microfluidics," *Electrophoresis*, vol. 42, no. 23, pp. 2538–2551, 2021.

[69] X. Jiang, W. Jing, L. Zheng, S. Liu, W. Wu, and G. Sui, "A continuous-flow high-throughput microfluidic device for airborne bacteria pcr detection," *Lab Chip*, vol. 14, no. 4, pp. 671–676, 2014.

[70] X. Jiang, W. Jing, X. Sun, Q. Liu, C. Yang, S. Liu, K. Qin, and G. Sui, "High-throughput microfluidic device for lamp analysis of airborne bacteria," *ACS Sens.*, vol. 1, no. 7, pp. 958–962, 2016.

[71] J. Jin, L. Duan, J. Fu, F. Chai, Q. Zhou, Y. Wang, X. Shao, L. Wang, M. Yan, X. Su, *et al.*, "A real-time lamp-based dual-sample microfluidic chip for rapid and simultaneous detection of multiple waterborne pathogenic bacteria from coastal waters," *Anal. Methods*, vol. 13, no. 24, pp. 2710–2721, 2021.

[72] M. Azizi, M. Zaferani, S. H. Cheong, and A. Abbaspourrad, "Pathogenic bacteria detection using rna-based loop-mediated isothermal-amplification-assisted nucleic acid amplification *via* droplet microfluidics," *ACS Sens.*, vol. 4, no. 4, pp. 841–848, 2019.

[73] J. R. Peham, W. Grienauer, H. Steiner, R. Heer, M. J. Vellekoop, C. Nöhammer, and H. Wiesinger-Mayr, "Long target droplet polymerase chain reaction with a microfluidic device for high-throughput detection of pathogenic bacteria at clinical sensitivity," *Biomedical Microdevices*, vol. 13, pp. 463–473, 2011.

[74] S. Choo, H. Lim, T. E. Kim, J. Park, K. B. Park, C. Park, C. S. Lim, and J. Nam, "A continuous microfluidic concentrator for high-sensitivity detection of bacteria in water sources," *Micromachines*, vol. 13, no. 7, p. 1093, 2022.

[75] L. D'Amico, N. Ajami, J. Adachi, P. Gascoyne, and J. Petrosino, "Isolation and concentration of bacteria from blood using microfluidic membraneless

dialysis and dielectrophoresis," *Lab Chip*, vol. 17, no. 7, pp. 1340–1348, 2017.

[76] S. Li, F. Ma, H. Bachman, C. E. Cameron, X. Zeng, and T. J. Huang, "Acoustofluidic bacteria separation," *J Micromech Microeng*, vol. 27, no. 1, p. 015031, 2016.

[77] P. Dow, K. Kotz, S. Gruszka, J. Holder, and J. Fiering, "Acoustic separation in plastic microfluidics for rapid detection of bacteria in blood using engineered bacteriophage," *Lab Chip*, vol. 18, no. 6, pp. 923–932, 2018.

[78] D. Puchberger-Enengl, S. Podszun, H. Heinz, C. Hermann, P. Vulto, and G. A. Urban, "Microfluidic concentration of bacteria by on-chip electrophoresis," *Biomicrofluidics*, vol. 5, no. 4, 2011.

[79] O. Schwartz and M. Bercovici, "Microfluidic assay for continuous bacteria detection using antimicrobial peptides and isotachophoresis," *Anal. Chem.*, vol. 86, no. 20, pp. 10106–10113, 2014.

[80] R. Wang, Y. Xu, T. Sors, J. Irudayaraj, W. Ren, and R. Wang, "Impedimetric detection of bacteria by using a microfluidic chip and silver nanoparticle based signal enhancement," *Mikrochim. Acta*, vol. 185, pp. 1–8, 2018.

[81] X. Wu, H. Wu, and Y. Hu, "Enhancement of separation efficiency on continuous magnetophoresis by utilizing l/t-shaped microchannels," *Microfluid. Nanofluidics*, vol. 11, pp. 11–24, 2011.

[82] N. Beyor, T. S. Seo, P. Liu, and R. A. Mathies, "Immunomagnetic bead-based cell concentration microdevice for dilute pathogen detection," *Biomed. Microdevices*, vol. 10, pp. 909–917, 2008.

[83] A. Munir, J. Wang, and H. Zhou, "Dynamics of capturing process of multiple magnetic nanoparticles in a flow through microfluidic bioseparation system," *IET Nanobiotechnol .*, vol. 3, no. 3, pp. 55–64, 2009.

[84] N. Xia, T. P. Hunt, B. T. Mayers, E. Alsberg, G. M. Whitesides, R. M. Westervelt, and D. E. Ingber, "Combined microfluidic-micromagnetic separation of living cells in continuous flow," *Biomed. Microdevices*, vol. 8, pp. 299–308, 2006.

[85] D. Rodoplu, C.-S. Chang, C.-Y. Kao, and C.-H. Hsu, "A simple magnetic-assisted microfluidic method for rapid detection and phenotypic characterization of ultralow concentrations of bacteria," *Talanta*, vol. 230, p. 122291, 2021.

[86] W. Lee, D. Kwon, W. Choi, G. Y. Jung, A. K. Au, A. Folch, and S. Jeon, "3d-printed microfluidic device for the detection of pathogenic bacteria using size-based separation in helical channel with trapezoid cross-section," *Sci. Rep.*, vol. 5, no. 1, p. 7717, 2015.

[87] W. Lee, D. Kwon, B. Chung, G. Y. Jung, A. Au, A. Folch, and S. Jeon, "Ultrarapid detection of pathogenic bacteria using a 3d immunomagnetic flow assay," *Anal. Chem.*, vol. 86, no. 13, pp. 6683–6688, 2014.

[88] J. Pivetal, S. Toru, M. Frenea-Robin, N. Haddour, S. Cecillon, N. M. Dempsey, F. Dumas-Bouchiat, and P. Simonet, "Selective isolation of bacterial cells within a microfluidic device using magnetic probe-based cell fishing," *Sens. Actuators B Chem.*, vol. 195, pp. 581–589, 2014.

[89] I. Pereiro, A. Bendali, S. Tabnaoui, L. Alexandre, J. Srbova, Z. Bilkova, S. Deegan, L. Joshi, J.-L. Viovy, L. Malaquin, *et al.*, "A new microfluidic approach for the one-step capture, amplification and label-free quantification of bacteria from raw samples," *Chem. Sci.*, vol. 8, no. 2, pp. 1329–1336, 2017.

[90] S. Miller, A. A. Weiss, W. R. Heineman, and R. K. Banerjee, "Electroosmotic flow driven microfluidic device for bacteria isolation using magnetic microbeads," *Sci. Rep.*, vol. 9, no. 1, p. 14228, 2019.

[91] C. H. Kim, J. Park, S. J. Kim, D.-H. Ko, S. H. Lee, S. J. Lee, J.-K. Park, and M.-K. Lee, "On-site extraction and purification of bacterial nucleic

acids from blood samples using an unpowered microfluidic device," *Sens. Actuators B Chem.*, vol. 320, p. 128346, 2020.

[92] L. Poncelet, L. Malic, L. Clime, M. Geissler, K. J. Morton, C. Nassif, D. Da Fonte, G. Veilleux, and T. Veres, "Multifunctional magnetic nanoparticle cloud assemblies for in situ capture of bacteria and isolation of microbial dna," *Analyst*, vol. 146, no. 24, pp. 7491–7502, 2021.

[93] H. Lee, G. Kim, E. Park, and S. Jeon, "Lenz's law-based virtual net for detection of pathogenic bacteria from water," *Anal. Chem.*, vol. 91, no. 24, pp. 15585–15590, 2019.

[94] H. Lee, H. Han, and S. Jeon, "Baleen-mimicking virtual filters for rapid detection of pathogenic bacteria in water using magnetic nanoparticle chains and a halbach ring," *ACS Sens.*, vol. 5, no. 11, pp. 3432–3437, 2020.

[95] F. Huang, H. Zhang, L. Wang, W. Lai, and J. Lin, "A sensitive biosensor using double-layer capillary based immunomagnetic separation and invertase-nanocluster based signal amplification for rapid detection of foodborne pathogen," *Biosens. Bioelectron.*, vol. 100, pp. 583–590, 2018.

[96] P.-D. Nguyen, T. B. Tran, D. T. X. Nguyen, and J. Min, "Magnetic silica nanotube-assisted impedimetric immunosensor for the separation and label-free detection of *Salmonella typhimurium*," *Sens. Actuators B Chem.*, vol. 197, pp. 314–320, 2014.

[97] J.-C. Yu, C.-C. Hu, W.-H. Chang, P.-C. Chen, M. S. Lee, K.-T. Peng, and G.-B. Lee, "An integrated microfluidic system using mannose-binding lectin for bacteria isolation and biofilm-related gene detection," *Microfluid. Nanofluidics*, vol. 22, pp. 1–10, 2018.

[98] U. Hatipoğlu, G. Kibar, and B. Çetin, "Enrichment of samples inside microchannels by using magnetic particles." Int. Patent Appl. No: PCT/TR2019/050728, 2019.

[99] U. Hatipoğlu, B. Çetin, and E. Yıldırım, "A novel zero-dead-volume sample loading interface for microfluidic devices: flexible hydraulic reservoir (fhr)," *J. Micromech. Microeng.*, vol. 28, no. 9, p. 097001, 2018.

[100] A. Atay, A. Topuz, B. Sarıarslan, E. Yıldırım, J. Charmet, K. Couling, and B. Çetin, "Flow rate-controlled pipetting for microfluidics: second-generation flexible hydraulic reservoir (fhrv2)," *Microfluid. Nanofluid.*, vol. 25, no. 1, p. 3, 2021.

[101] S. D. Minteer, *Microfluidic techniques: reviews and protocols*, vol. 321. Springer Science & Business Media, 2008.

[102] Y. Kwon, C. A. Hara, M. G. Knize, M. H. Hwang, K. S. Venkateswaran, E. K. Wheeler, P. M. Bell, R. F. Renzi, J. A. Fruetel, and C. G. Bailey, "Magnetic bead based immunoassay for autonomous detection of toxins," *Anal. Chem.*, vol. 80, no. 22, pp. 8416–8423, 2008.

[103] J.-W. Choi, T. M. Liakopoulos, and C. H. Ahn, "An on-chip magnetic bead separator using spiral electromagnets with semi-encapsulated permalloy," *Biosens. Bioelectron.*, vol. 16, no. 6, pp. 409–416, 2001.

[104] S. Guo, Y. Deng, L. Zhao, H. Chan, and X. Zhao, "Effect of patterned micro-magnets on superparamagnetic beads in microchannels," *Journal of Physics D: Applied Physics*, vol. 41, no. 10, p. 105008, 2008.

[105] G. Kibar, A. E. Topal, A. Dana, and A. Tuncel, "Newly designed silver coated-magnetic, monodisperse polymeric microbeads as sers substrate for low-level detection of amoxicillin," *J. Mol. Struct.*, vol. 1119, pp. 133–138, 2016.

[106] G. Kibar, "Effect of crosslinking agent on mesoporous spherical poss hybrid particles: Synthesis, characterization and thermal stability," *J Inorg Organomet Polym Mater*, vol. 33, no. 3, pp. 831–840, 2023.

[107] G. Günal, Ç. Kip, S. E. Öğüt, D. D. Usta, E. Şenlik, G. Kibar, and A. Tuncel, "Human genomic dna isolation from whole blood using a simple microfluidic system with silica-and polymer-based stationary phases," *Mater. Sci. Eng. C*, vol. 74, pp. 10–20, 2017.

[108] G. Kibar and D. Ş. Ö. Dinç, "In-situ growth of ag on mussel-inspired polydopamine@ poly (m-poss) hybrid nanoparticles and their catalytic activity," *J. Environ. Chem. Eng.*, vol. 7, no. 5, p. 103435, 2019.

[109] H. Modh, T. Scheper, and J.-G. Walter, "Aptamer-modified magnetic beads in biosensing," *Sensors*, vol. 18, no. 4, p. 1041, 2018.

[110] H. P. Khng, D. Cunliffe, S. Davies, N. A. Turner, and E. N. Vulfson, "The synthesis of sub-micron magnetic particles and their use for preparative purification of proteins," *Biotechnol. Bioeng.*, vol. 60, no. 4, pp. 419–424, 1998.

[111] T. Chen, Y. Xu, and J. Li, "Recent advances in electrochemical impedance spectroscopy-based pathogenic bacteria sensing," *Int J Electrochem*, p. 0, 2023.

[112] L. Yang, Y. Li, and G. F. Erf, "Interdigitated array microelectrode-based electrochemical impedance immunosensor for detection of *Escherichia c oli O157: H7*," *Anal. Chem.*, vol. 76, no. 4, pp. 1107–1113, 2004.

# Appendix A

# Fabrication recipe

## A.1 Mold fabrication steps

This recipe enables users to produce SU-8 structures with a thickness of 120 µm on a 4-inch Silicon (100) wafer with a thickness of 0.5 mm. To modify the height of the structures, you can spin coating speed can be changed based on data provided in the SU-8 datasheet.

**Part 1 (Cleaning and Preparation)**

- Wash the wafer with Acetone followed by IPA, then DI water.
- Place in oven at 120°C for 2 mins to remove residual water,

**Part 2 (Base Layer: SU8-2005 (Negative photoresist))**

- Dispense 4 mL of resist on a substrate.
- Set the two-step spin coating parameters at (A) a velocity of 500 rpm and acceleration of 100 rpm/s for 7 s, followed by (B) Spinning at 2000 rpm

with an acceleration of 300 rpm/s for 30 s.

- Do edge bead Removal with an acetone-soaked napkin.
- Soft bake it on a hot plate at 95°C for 3 min.
- Espouse whole Wafer using Mask Aligner without mask using the listed parameters:
  Manual top side, Contact mode = Soft contact, Separation = 50 μm, Mask thickness = 2.3 mm, Sample thickness = 0.5 mm, Resist thickness = 7 μm, UV intensity = 140 mJ/cm$^2$
- Post-exposure Bake the substrate on a hot plate at 95°C for 4 min.

**Part 3 (Main Layer: SU8-2050 (Negative photoresist))**

- Dispense 4 mL of resist on a substrate.
- Set the two-step spin coating parameters at (A) a velocity of 500 rpm and acceleration of 100 rpm/s for 7 s, followed by (B) Spinning at 1200 rpm with an acceleration of 300 rpm/s for 30 s.
- Do edge bead removal with an acetone-soaked napkin.
- Soft bake it on a hot plate at 65°C for 3 min, followed by 25 min of baking at 95°C and 2 min at 65°C.
- Espouse whole wafer using Mask Aligner with a designed mask using the listed parameters:
  Manual top side, Contact mode = Soft contact, Separation = 200 μm, Mask thickness = 2.3 mm, Sample thickness = 0.5 mm, Resist thickness = 150 μm, UV intensity = 340 mJ/cm$^2$
- Post-exposure bake the substrate on a hot plate at 65°C for 3 min, followed by 10 min of baking at 95°C and 2 min at 65°C.

**Part 4 (Development)**

- After cooling the wafer, drown it in SU-8 developer and agitate it slowly for 9 mi.
- Wash the developed image with IPA and DI water.
- Examine the wafer, and if necessary, develop it for an additional minute.
- Dry with pressurized nitrogen.

## A.2 Electrode fabrication steps

This recipe enables users to fabricate the electrodes with the desired thickness (usually 80 nm to 100 nm) on a 4-inch glass wafer.

**Part 1 (Cleaning and Preparation)**

- Wash the wafer with Acetone followed by IPA, then DI water.
- Place in oven at 120°C for one minute to remove residual water,

**Part 2 (Photolithography)**

- Dispense 4 mL of resist on a substrate.
- Spin coat AZ 5214 with setting parameters at 2200 rpm and acceleration of 100 rpm/s for 40 s .
- Bake it in the oven at 120°C for 70 seconds.
- Espouse whole Wafer using Mask Aligner with a designed mask for electrodes using the listed parameters:
  Manual top side, Contact mode = V+H mode (Don't forget to increase

the pressure and use circular plastic on the plate for vacuum), Separation: 100 μm, Substrate thickness: 0.5 mm (measure it for your wafer), Resist thickness: 2 μm, **Exposure intensity:** mJ/cm$^2$

**Part 4 (Development)**

- After cooling the wafer, drown it Water: 400K (4:1) for 30 s. Very slow stirring.
- Wash the developed image with DI water for 30 s.
- Dry wafer with $N_2$ and check the pattern under the microscope. If the pattern is not developed yet, develop 5-10 s more.

**Part 5 (Thermal Evaporation For Chromium and Gold Deposition )**

- Deposit Chromium to reach the thickness of 0.03 kA° (3nm), Tooling Factor: 77, Power: 55-77 at a rate of less than 0.3 (A°/s).
- Deposit Gold to reach the thickness of 1 kA° (100 nm) Tooling Factor: 150, Power: 150-200 at a rate of less than 0.5 (A°/s).
- Place the wafer in Acetone for 24 h or more (need to check).